Recursive interaction between encapsulated dynamic microtubule asters and deformable membranes

Dissertation

Zur Erlangung des akademischen Grades eines

Doktors der Naturwissenschaften

(Dr. rer. nat.)

der Fakultät Chemie und Chemische Biologie

der Technischen Universität Dortmund

vorgelegt von

Farid Ghasemalizadeh

von Farid Ghasemalizadeh

Gutachter:

Prof. Dr. Philippe Bastiaens

Prof. Dr. Leif Dehmelt

The work presented in this dissertation was performed in the laboratory of Prof. Dr. Philippe Bastiaens at the Max Planck Institute of Molecular Physiology, Dortmund, Germany.

“Hombruch boyz, ASSEMBLE”

-FADAAW

Table of Contents

1-Abstract **8**

1-Zusammenfassung **10**

2-Introduction **13**

2.1-Microtubules **13**

2.2- Structure of microtubules **15**

2.3- The origin of dynamic instability **17**

2.4-Microtubule associated proteins (MAPs) **18**

2.5-Stathmin / op18 ..... **19**

2.6-Lipid bilayer structure and its interaction with microtubules **20**

3-Objectives **23**

4-Results **25**

4.1- The effect of tubulin concentration and stathmin phosphorylation state on microtubule dynamics **25**

4.2-The effect of tubulin concentration and stathmin phosphorylation on the size of microtubule asters **30**

4.3-Microtubule-asters reorganizing themselves in response to their dynamics in deformable confinement **33**

4.4-recursive interaction between cytoskeleton and signaling gradient in deformable membrane: Synthetic Morphogenic Membrane System (SynMMS) **37**

5-Disscussion **46**

6-Materials and Methods **50**

6.1-Preparation and labeling of tubulin **50**

6.2-Preparation of centrosomes **53**

6.3-Protein encapsulation in GUVs by cDICE 54

6.4-Imaging of MT asters and morphological states in GUVs 55

6.5-Single-filament TIRF-M assay and data analysis 57

6.6-Determination of MT-aster size *in vitro* 58

7-References 60

8-Acknowledgement 72

1-Abstract

Cytoskeletal networks, the filamentous systems in the cytoplasm of cells, are giving the cell its shape and supporting the mechanical structure of the cell, as well as organizing the cytoplasmic organelles in the cell. The cytoskeleton microtubules are reorganizing and maintaining the global morphology of the cell. This is the result of the signals that regulate microtubule filaments. The geometry of the membrane also affects these signaling pathways, which leads to the recursive interaction of the microtubules and signals at the membrane. To reconstitute a minimal system for the purpose of studying this recursive interaction, purified pig brain tubulin together with purified centrosomes, as microtubule organizing centers, was encapsulated in giant unilamellar vesicles (GUVs) using the cDICE method (Abkarian et al., 2011). To study how microtubule dynamics is regulated by tubulin concentration, different concentrations of tubulin dimers, with and without different concentrations of the microtubule regulator stathmin (Daub et al., 2001) in both unphosphorylated and phosphorylated states, were used for single filament TIRF microscopy (Bieling et al., 2010) to study the microtubule dynamics, as well as confocal laser scanning microscopy (CLSM) to investigate the effect of regulators and confinement on the microtubule asters. For further investigation of the effect of a phosphorylated stathmin gradient on the positioning of microtubule asters and the morphology of GUVs, dynamic microtubule asters were encapsulated together with a signaling system which mimics the Rac1-Pak1 pathway that controls the microtubule regulator stathmin (Daub et al., 2001).

Stathmin sequesters tubulin dimers, thus decreasing the effective concentration of tubulin, which affects microtubule dynamics. This inhibitory effect of stathmin is regulated by its phosphorylation. As a result, the size of microtubule asters is smaller in the presence of stathmin as compared to the phosphorylated stathmin. This results in the reorganization of microtubule asters in confinement. Introducing the light-activated phosphorylated stathmin gradient in the system, which forms upon kinase translocation to the membrane, shows: the pre-formed microtubule based protrusions are stable, newly formed protrusions are caused

by the signaling system and the response of the system to the activation of the signaling system depends on the initial morphology of the confinement.

1-Zusammenfassung

Zytoskelettnetzwerke, die filamentösen Systeme im Zytoplasma von Zellen, verleihen der Zelle ihre Form und unterstützen die mechanische Struktur der Zelle sowie die Organisation der zytoplasmatischen Organellen. Die Zytoskelett-Mikrotubuli reorganisieren und unterstützen die globale Morphologie der Zelle. Dies ist das Ergebnis der Signale, die die Mikrotubuli-Filamente regulieren. Die Geometrie der Plasmamembran beeinflusst auch diese Signalwege, was zu einer rekursiven Wechselwirkung der Mikrotubuli und der Signale an der Membran führt. Um ein Minimalsystem für die Untersuchung dieser rekursiven Wechselwirkung zu rekonstituieren, wurde gereinigtes Schweinegehirn-Tubulin zusammen mit gereinigten Centrosomen als Organisationszentren von Mikrotubuli in unilamellaren Riesenvesikeln (GUVs) unter Verwendung der cDICE-Methode eingekapselt (Abkarian et al., 2011). Um zu untersuchen, wie die Mikrotubulidynamik durch die Tubulinkonzentration reguliert wird, wurden unterschiedliche Konzentrationen von Tubulindimeren mit und ohne unterschiedliche Konzentrationen des Mikrotubuli-Regulators Stathmin (Daub et al., 2001) sowohl im unphosphorylierten als auch im phosphorylierten Zustand für die Einzelfilament-TIRF-Mikroskopie verwendet (Bieling et al., 2010), sowie konfokale Laserscanningmikroskopie (CLSM) zur Untersuchung der Wirkung von Regulatoren und der Enkapsulierung auf die Mikrotubuliaster. Zur weiteren Untersuchung der Auswirkung eines phosphorylierten Stathmin-Gradienten auf die Positionierung von Mikrotubuliastern und der Morphologie von GUVs wurden dynamische Mikrotubuliaster zusammen mit einem Signalsystem enkapsuliert, das den Rac1-Pak1-Signalweg nachahmt, der den Mikrotubuli-Regulator Stathmin reguliert (Daub et al (2001).

Stathmin bindet Tubulindimere und senkt so die effektive Konzentration von Tubulin, was die Dynamik der Mikrotubuli beeinflusst. Diese hemmende Wirkung von stathmin wird durch seine Phosphorylierung reguliert. Als Ergebnis ist die Größe der Mikrotubuliaster in Gegenwart von Stathmin im Vergleich zu dem phosphorylierten Stathmin verringert. Dies führt zur Umorganisation von Mikrotubuliastern in GUVs. Das Anschalten des lichtaktivierten phosphorylierten Stathmin-Gradienten in dem System, der sich bei Kinasetranslokation zur

Membran bildet, zeigt: die vorgeformten, auf Mikrotubuli basierenden Ausstülpungen sind stabil, neu gebildete Ausstülpungen werden durch das Signalsystem und die Interaktion des Systems mit der Membran verursacht, wobei diese Interaktion von der ursprünglichen Morphologie der GUVs abhängt.

2-Introduction

Cells are able to sense and adapt their functions to the environmental changes by generating motility or reorganizing their microfilament-supported shape and morphology. These responses are originated from signaling pathways that regulate microfilament dynamics (Mitchison and Kirschner, 1984) via regulator molecules. These microfilament dynamic networks, which are called cytoskeleton, have evolved in eukaryotic cells efficiently to enable fast rearrangement and adaptation to the regulatory signals. The diverse functions of the cytoskeleton, including the maintenance of the cell shape and position of the organelles, are directly connected to three filamentous networks: actin microfilaments, intermediate filaments, and microtubules. Microtubules are the main filaments to generate, support and maintain the global shape of the cells.

2.1-Microtubules

Microtubules were identified to form the mitotic spindle (Schmidt, 1939) and later on, Inoue and Dan showed that the spindles are composed subunits, which can assemble and disassemble to form a dynamic structure (Inoué & Dan, 1951). Since then, with the help of technical improvements in microscopy and biochemistry, there was tremendous progress in understanding the structure of microtubules and their involvement in many cellular functions.

Microtubules are hollow filamentous protein polymers, with a diameter of 25 nm that can be found in all eukaryotic cells (Figure.1-1). These filaments are highly dynamic and, similar to the other cytoskeletal components, serve to spatially organize the cytoplasmic space by emanating from a microtubule organizing center, also known as centrosome, towards the periphery. Being a part of cytoskeletal dynamic networks, microtubules are necessary for maintaining cell shape and stability (Conde & Caceres, 2009, Verhey & Gaertig, 2007). But the function of the microtubule network is more than only serving as an intracellular skeleton.

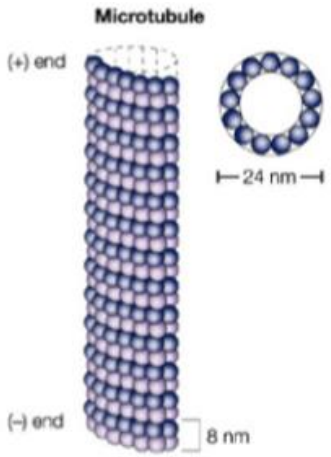

Figure.1-1 Structure of microtubules. Tubulin dimer is polymeryzing into microtubules. In microtubules, nucleation is followed by elongation on both ends to form a cylinder with a diameter of 25 nm and arranged in a head-to-tail fashion in 13 protofilaments (Scheme modified from Wilson, 2004).

During cell division, microtubules originate from two organizing centers and extend towards the chromosomes, forming the mitotic spindle in order to properly segregate the chromosomes (Susane et al., 2004). It is important to understand that the assembly and disassembly of the mitotic spindle is originated by changes in microtubule dynamics (Gouveia & Akhmanova, 2010).

Also, cargos need to be transported over long distances, where microtubules are serving as tracks for many different vesicles and organelles (Caviston & Holzbaur, 2006, Hirokawa, 1998) with the help of motor proteins (Hirokawa et al., 2010). This function is especially important in neurons where axons can be one meter long and diffusion is not significantly efficient to transport proteins (S. Rogers et al., 2000) Microtubules also play an important role in cell polarity (Neukirchen & Bradke, 2011), especially during interphase, where microtubules are providing tracks for organelles localization and stability of the cell polarity (A. Muensch, 2007).

Moreover, microtubules support and maintain the mechanical stability of the cell shape. It is important to keep in mind that microtubules being highly dynamic is an important aspect for their function. The best example to show the effect of being highly dynamic is exposing dividing cells to the microtubule stabilizing drugs, such as taxol, where the microtubules are unable to depolymerize and in a result they can not pull the chromosomes during mitosis (M. Jordan and L. Wilson, 2004).

Microtubules are constantly switching phases between polymerization and

depolymerization. Mitchison and Kirschner called this behavior dynamic instability of microtubules (M. Carlier et al., 1981, Mitchison and Kirschner, 1984), and it was observed both in vitro and in vivo (Mitchison and Kirschner, 1984, Fygenson, 1994). Dynamic instability enables microtubules to explore the cellular space continuously which is necessary to bring microtubules in contact with cytosolic compartments as well as adapting the shape of the cell to the changes in the environment (Mitchison and Kirschner, 1984, T. Hill, 1985, T. Holy et al.,1994, R. Wollman et al., 2005).

2.2- Structure of microtubules

To study the effect of dynamic microtubules in cellular context, a better understanding of microtubule composition is required (Figure.1-1). Microtubules are non-covalent polymers of stable α-β tubulin dimers. These subunits are polymerizing in a head-to-tail fashion and build a polar filament with two functionally different ends. The α-tubulin subunit is oriented towards the minus-end whereas the β-tubulin subunit is oriented towards the plus-end (Conde & Caceres, 2009, Desai & Mitchison, 1997, Nogales, 2000). Both subunits are similar at the sequence level and have the ability to bind Guanosine-5'-triphosphate (GTP). The binding site is known as N-site in α-tubulin subunit and is non-exchangeable, where in the β-tubulin subunit, the binding site in known as E-site and is exchangeable (E. Nogales, 1998, Noda et al., 2012). β-tubulin has an intrinsic GTPase activity. During microtubule polymerization, addition of α-β tubulin dimer causes the catalytic domain of the α-tubulin to contact the E-site in the β-tubulin of the previously added α-β tubulin dimer, enabling GTP hydrolysis. After GTP is hydrolyzed to Guanosine-diphosphate (GDP), it can be exchanged for a new GTP molecule once the microtubule is depolymerized and the α-β tubulin dimer is released to the cytosol (Figure.1-2).

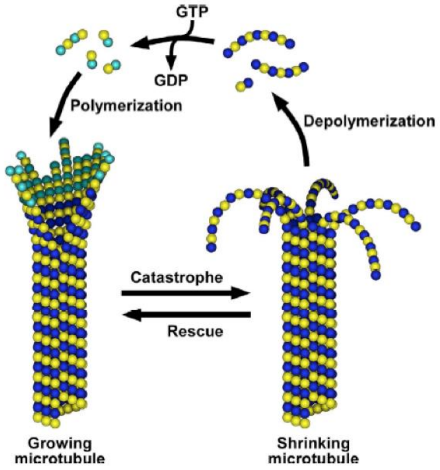

Figure.1-2 Microtubule dynamics. Binding, hydrolysis and the GTP/GDP exchange in the β-tubulin monomer is causing the growing microtubule to undergo depolymerization. On the other hand, addition of GTP-bound tubulin promotes polymerization. Constant interchange of these two phases is called dynamic instability (Scheme modified from Akhmanova and Steinmetz, 2008).

GTP-bound tubulin (the E-site contains GTP) has a straight structure and therefore polymerize into the growing microtubule. After polymerization, there is a delay after which hydrolysis takes place. GDP-bound tubulin (hydrolysis of GTP to GDP in the E-site) changes the structure of α-β tubulin dimer into a lightly bent structure, which promotes the depolymerization of the microtubule (E. Nogales et al., 2006). This delay causes a layer of GTP-bound tubulin at the plus end of the microtubule, so called GTP-cap, which stabilizes the microtubule lattice (Akhmanova & Steinmetz, 2011, Conde & Caceres, 2009). So, the microtubule lattice is mainly consisting of GDP-bound tubulin except the tip of the microtubule where the GTP-cap exists, which describes two main characteristics of microtubules, their dynamics and their polarity (Downing & Nogales, 1998b).

2.3- The origin of dynamic instability

Dynamic microtubules undergo rapid changes between growth, pause and shrinkage according to dynamic instability of microtubules (Mitchison & Kirschner, 1984) (Figure.1-2). The transition from depolymerization to polymerization is called "rescue", where the transition from polymerization to depolymerization is called "catastrophe" (Noda et al., 2012). Experiments *in vivo* and *in vitro* have shown this behavior (Conde & Caceres, 2009, Gouveia & Akhmanova, 2010). Microtubules are undergoing catastrophe by losing the GTP-cap which leads to a sudden exposure of GDP-subunits from the plus end, resulting in splaying apart of the microtubule and formation of a fountain-like structure (Akhmanova & Hoogenraad, 2005, Akhmanova & Steinmetz, 2008, Conde & Caceres, 2009). On the other hand, rescue depends on the free tubulin dimer concentration (Akhmanova & Hoogenraad, 2005, Walker et al., 1988). *In vivo* studies show that rescue can be due to the remaining of GTP-bound tubulin in the microtubule lattice (Gardner et al., 2013).

To describe the dynamics of microtubules, four parameters are defined: the growth velocity (V_g), the shrinkage rate (V_s), the catastrophe frequency (f_{cat}) and the rescue frequency (f_{res}). These parameters can be independently regulated by microtubule associated proteins (MAPs) or other regulatory factors (Conde & Caceres, 2009).

Microtubule dynamics was also studied in the presence of nucleotide analogues, in particular GMPCPP. In this case, GMPCPP is resistant to the intrinsic GTPase activity of tubulin dimer, resulting in a microtubule lattice that is unable to undergo catastrophe (A, Hyman et al., 1992).

But dynamic behavior of microtubules is not only regulated by free tubulin concentration or GTP hydrolysis, but is also controlled by multiple other factors, such as posttranslational modifications or microtubule associated proteins (Conde & Caceres, 2009).

2.4-Microtubule associated proteins (MAPs)

Microtubules were found to be accompanied with additional proteins, so called microtubule associated proteins, that can alter the microtubule dynamics. MAPs are playing an important role in stabilizing or destabilizing microtubules and involved in cross-linking microtubules with each other and other filamentous networks. MAPs are generally consisting of conserved carboxyl-terminated domain containing microtubule-binding site and an amino-terminal projection domain of different size (Dehmelt and Halpain, 2004).

MAPs can globally affect the microtubule dynamics. For example, during transition from interphase to mitosis, microtubule arrays, which are longer in interphase than mitosis, need to undergo catastrophe with almost tenfold lower frequencies. MAPs can either act on tubulin subunit level by promoting or suppressing polymerization, or interact directly with microtubule lattice, stabilizing or destabilizing the microtubule.

MAPs can also locally affect microtubule dynamics. The existence of a steady-state gradient of regulatory activities, such as a gradient of Ran-GTP (Carazo-Salas, Guarguaglini, et al. 1999, Kalab, Pu et al., 1999) has been thought to be the cause of polarized growth. In the vicinity of mitotic chromatin, due to the activity of the nucleotide exchange factor (GEF) RCC1, the small GTPase Ran, which is localized on the chromosome, is continuously loaded with GTP. In addition to the opposing activity of cytoplasmic GTPase activating protein (Ran-GAP) that inactivates Ran, leads to steady-state gradient of GTPase activity (Kalab, Weis et al. 2002, Caudron et al., 2005). In addition to Ran gradient, activity of the microtubule destabilizing protein, stathmin/op18, has been thought to exist in the vicinity of mitotic chromatin (Andersen, Ashford et al., 1997, Budde, Kumagai et al., 2001). This gradient has the ability to promote the microtubule growth by lowering the catastrophe frequency leading to growth of microtubules that approach the chromosomes, while the catastrophe frequency is higher in the other directions (Niethammer et al., 2004, 2007).

2.5-Stathmin / op18

Stathmin is a member of microtubule destabilizing regulators. Stathmin is affecting microtubule dynamics by promoting catastrophe during interphase and late mitosis. This activity is regulated by the stathmin phosphorylation. These modifications are important factors to regulate the microtubule dynamics during different phases of the cell cycle.

Stathmin is an 18 kD protein (Brattsand et al., 1993). Originally, Stathmin was described by binding to tubulin dimers (Belmont et al., 1996) forming a complex T_2S, containing two tubulin dimers (Belmont and Mitchison, 1996). The inhibitory activity of stathmin is hypothesized with two different mechanisms: sequestering tubulin dimers that affect microtubule growth velocity (Jourdain et al., 1997; Curmi et al., 1999) or promoting catastrophe by directly affecting the microtubule lattice (Tournebize et al., 1997; Segerman et al., 2003). The sequestering mechanism was shown by structural and biophysical studies (Steinmetz et al., 2000; Gigant et al., 2000; Wallon et al., 2000; Muller et al., 2001; Charbaut et al., 2001; Amayed et al., 2002). *In vitro*, it was shown that at a pH of 6.8, stathmin binds to two tubulin dimers forming and sequesters tubulin from the tubulin pool (Cassimeris, 2002), whereas at a pH of 7.5, stathmin promotes catastrophes by directly interacting with growing microtubule end and promoting depolymerization (Howell et al., 1999a).

Stathmin is active in its unphosphorylated state. However, stathmin is phosphorylated at four serine residues (Ser 16, 25, 38 and 63) by both cell-regulating and signal-transducing kinase systems (Lawler, 1998), which results in the inactivation of stathmin regulatory activity (Marklund et al., 1996; Larsson et al., 1997; Horwitz et al., 1997). Phosphorylation of stathmin at different sites is necessary during mitosis for the formation of spindle (Larsson et al., 1997). Phosphorylation of Ser16 and Ser63significantly reduces the affinity of stathmin to tubulin, which affects the microtubule dynamics (Di et al., 1997; Holmfeldt et al., 2001). This inhibition is furthermore affected by phosphorylation on Ser25 and Ser38 (Antonsson et al., 1998). PKA, MAP kinases and CDKs, which are highly expressed in neurons and also present in growth cones, are known to regulate the inhibitory activity of stathmin *in vivo* (Pigino et al., 1997).

2.6-Lipid bilayer structure and its interaction with microtubules

Cell are enclosed by a plasma membrane, composed of different lipids and proteins, which builds up a 6 nm to 10 nm thick two-dimensional bilayer, and acts not only as a barrier to maintain the physical integrity of the cell, but also is involved in many cellular function such as cell signaling, motility and cellular adhesion (K. Karen et al,. 2005).
The plasma membrane can be seen as a multilayer system (B. Alberts et al., 2008). The outer layer is formed from the glycolipid and the branched polypeptide of the glycoproteins' head groups (S. Reitsma, 2007, W. Weinbaum, 2007), and the inner layer is made of cytoskeleton microfilaments (B. Head et al., 1996). The middle layer is formed by the lipid-protein structure held together by non-covalent bonds (K. Boesze et al., 1997, Coskun and Simon, 2011). The composition of the central layer varies from cell type to another, but cells maintain the same few classes of lipids from the enormous variety of natural occurring lipids, mainly consisting of phospholipids; phosphatidylcholine (PC), phosphatidylserine (PS), phosphatidylethanolamine (PE), sphingomyelin (SPHM). (G. can Meer et al., 2008).
Plasma membrane also anchors to the cytoskeleton in order to maintain the cell shape, thus understanding the properties of the membrane is necessary. The interaction between the three-dimensional cytoskeleton network and two-dimensional lipid membrane is a key feature of the cell functions. Cells reorganize and adapt their shape, which is supported by cytoskeleton, during exposure to the morphogen signals. This response is based on the signaling pathways regulating cytoskeleton dynamics (Mitchison and Kirschner, 1984). During changing the shape of the cell, signaling is actuated via dimensionality reduction (Adam and Delbrück, 1968, Oancea and Meyer, 1998, Shen and Meyer, 1999) where the local concentration of the regulators are increased in the vicinity of the plasma membrane. This leads to the higher activity of the cytoskeleton regulators at the plasma membrane comparing to the cytosolic activity, which results to the cytoskeleton to be directed locally towards the membrane (Niethammer et al., 2004, 2007). Changing the shape of the membrane affects the local concentration of the translocated molecules on the membrane, resulting the increased activity of the signaling reactions (Rangamani et al., 2013). Since the dynamic microtubules are able to deform the membrane, they are exposed to the signaling reactions, which regulate their dynamic, results in autocatalytic amplification that affects the dynamic microtubules, which are self-organized in the confinement (plasma

membrane) (Schmick 2014). This recursive interaction constantly adapting the shape of the cell to the extracellular cues as well as to the previous shape of the cell.

In order to study protein-protein interactions in a confinement, three-dimensional water-in-water lipid vesicles are usually used to encapsulate proteins inside a cell-like membrane. The structure of the membrane depends on the formation techniques, and they can have a single bilayer (unilamellar) or multi-bilayer (multilamellar) (C. McPhee et al., 2013). Considering the size of the formed lipid vesicles, they are categorized into: small unilamellar vesicles (SUVs) with the size of smaller than 100 nm, large unilamellar vesicles (LUVs) with the size of 100 nm and few micrometers, and giant unilamellar vesicles (GUVs) with the size of larger than 5 micrometers (Schmitt et al., 2016). Because of the large size of GUVs, they are widely used in synthetic biology studies (P. Mueller et al., 1983, P. Walde et al., 2010).

3-Objectives

Cells rearrange their cytoskeleton-based morphology in response to the extracellular signals that regulate the cytoskeleton dynamics, and this response leads to morphological changes. Extracellular signals regulate the cytoskeleton dynamics via regulators that diffuse in the cytoplasm (Daub et al., 2001). However, the confinement that interacts with dynamic cytoskeleton and the regulators, constrains both cytoskeleton and the regulator molecules. Due to the universal mechanism of dimensionality reduction (Adam and Delbrück, 1968, Oancea and Meyer, 1998, Shen and Meyer, 1999), signaling activity is enhanced at the membrane of the confinement compared to the cytosolic activity of the regulatory molecules, thus affecting cytoskeletal filaments locally at the membrane via a dynamically maintained gradient of regulators (Niethammer et al., 2004, 2007). However, the geometry of the membrane affects the local concentration of the regulators (Rangamani et al., 2013). Studies have shown that that polarity emerges upon interaction between dynamic microtubules and motor proteins (Baumann and Surrey, 2014, Juniper et al., 2018, Laan et al., 2012, Letort et al., 2016, Nédélec et al., 1997, Pinot et al., 2009, Surrey et al., 2001). The question is how the morphology and the overall shape of the cell result from recursive interaction between dynamic microtubules and the signaling at the membrane of the cell. To answer this question, in this study, a minimal cytoskeletal system is encapsulated together with a light-inducible membrane-based signaling system in Giant Unilamellar Vesicles (GUVs).

4-Results

4.1- The effect of tubulin concentration and stathmin phosphorylation state on microtubule dynamics

To study the effect of tubulin and stathmin concentration on the microtubule dynamics, Total Internal Reflection Fluorescence microscopy (TIRF) was used. In this assay, immobilized GMPCPP-stabilized microtubule-seeds (20 % Alexa568-tubulin, 5 % Biotin-tubulin) on the Biotin-PEG glass surface were used as polymerization sites for dynamic microtubules (Figure.2-1).

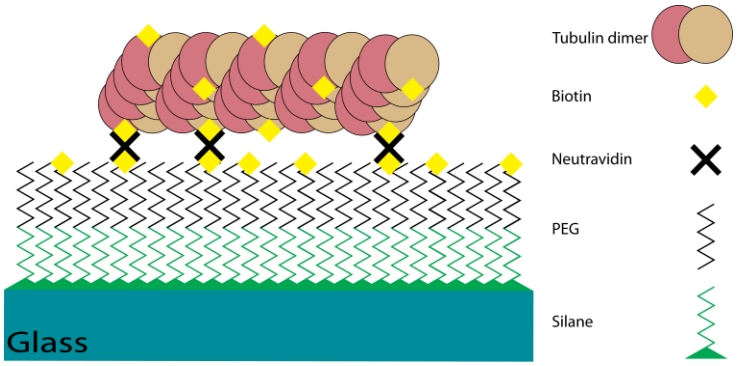

Figure.2-1 Immobilized GMPCPP-stabilized microtubule seeds. Slowly hydrolysable GTP analogue, GMPCPP, was used to polymerize tubulin into stabilized microtubules. The Biotin-PEG glass was used to immobilized microtubules on the surface for the TIRF assay.

In order to investigate the effect of tubulin concentration on the microtubule dynamics, different tubulin concentrations (10% Alexa568-tubulin) were used. Higher ratio of labeled tubulin during polymerization of GMPCPP-stabilized microtubule seeds was used in order to distinguish the seed from the dynamic microtubule (Figure.2-2 A and B). To measure growth velocity and catastrophe frequency, kymographs (time-space plots) of the dynamic microtubules were used. Kymographs are a straightforward tool to measure the growth velocity. The slope of the kymograph shows the growth velocity (μm/min). The average number of catastrophe events in the period of the time was used to measure catastrophe frequency (1/sec). Upon increasing the tubulin concentration, the microtubule growth velocity was linearly increased. On the other hand, catastrophe frequency was decreased nonlinearly as a result of increasing tubulin concentration (Figure.2-2 C).

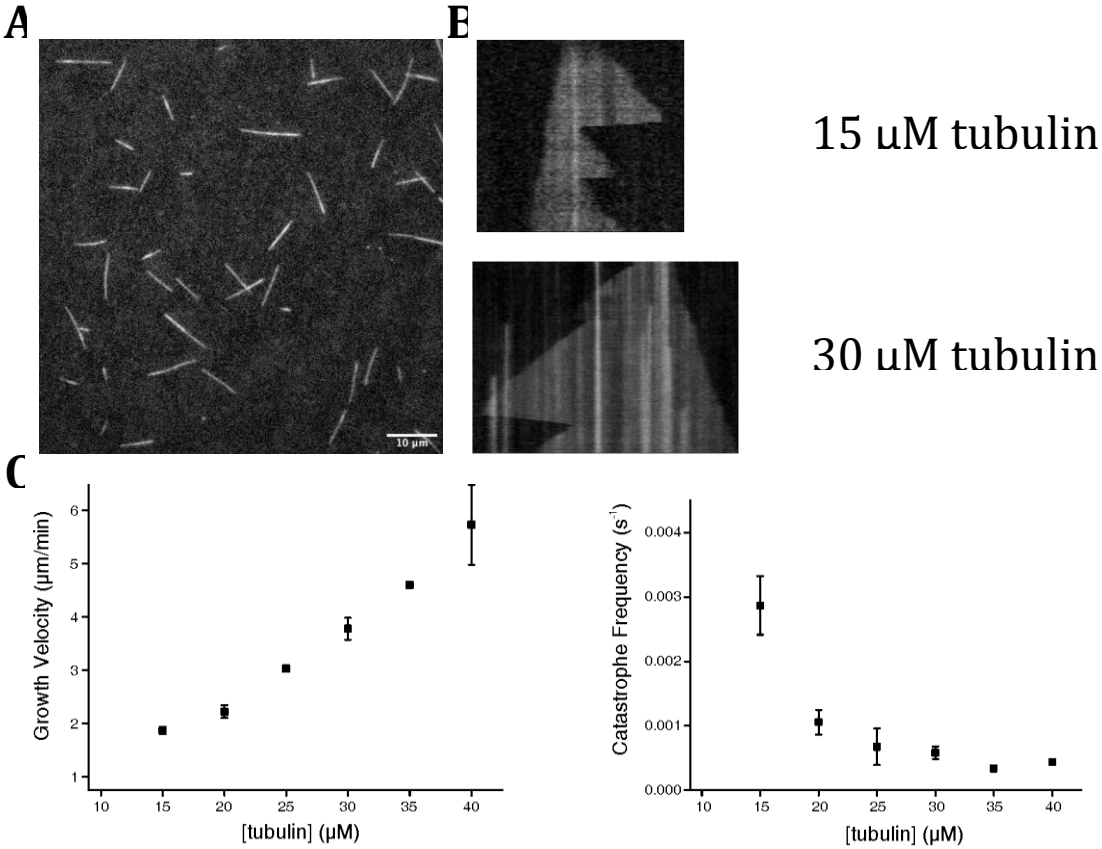

Figure.2-2 Microtubule dynamics. Microtubule dynamics depends on tubulin concentration. **(A)** an example of an image from a time-series obtained with TIRF microscopy with 15 µM tubulin after 6 minutes of polymerization. GMPCPP-stabilized seeds are brighter than dynamic microtubules. **(B)** kymographs of microtubules with 15 (top) and 30 (bottom) µM tubulin. The catastrophe events are identified by depolymerization of microtubules from GMPCPP-stabilized seeds. **(C)** Growth velocity was increased (left graph) and catastrophe frequency was decreased (right graph) in response to higher tubulin concentrations (error bars correspond to S.E.M, N > 75 tracked filaments)

To study the effect of stathmin on the microtubule dynamics, different concentrations of stathmin were introduced at high tubulin concentration (40 μM tubulin). As a result, the microtubule growth velocity was decreased. At 20 μM stathmin, no growing microtubules were observed. Additionally, the catastrophe frequency was increased in response to increasing stathmin concentration. To determine the effective tubulin concentration in the presence of stathmin, it was assumed that each stathmin molecule is binding to two tubulin dimers. Considering this assumption, it was concluded that stathmin is sequestering tubulin as we observed in the experiments (Figure.2-3). In the set of experiment with Alexa647-Stathmin was used to observe whether the stathmin is directly interacting with the tip of the growing microtubules or not. As a result, no Stathmin-comet was observed which shows that stathmin is only sequestering tubulin.

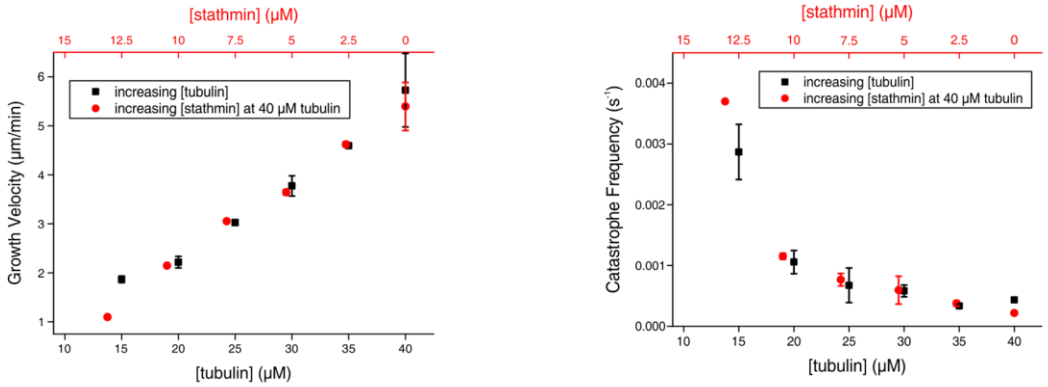

Figure.2-3 Microtubule dynamics in the presence of stathmin. Increasing stathmin concentration decreases growth velocity in a linear manner (left graph) and increases catastrophe frequency nonlinearly (right graph) (error bars correspond to S.E.M).

The stathmin-tubulin affinity is affected by stathmin phosphorylation. To investigate this effect on the microtubule dynamics, Protein kinase A (PKA) was used to phosphorylate stathmin. It is known that PKA phosphorylates stathmin on serine 16, 25, 38 and 63 (PKA consensus sites). By introducing different concentrations of phosphorylated stathmin into the system at high tubulin concentration (40 μM tubulin), growth velocity was decreased by increasing phospho-stathmin concentration, and the catastrophe frequency was increased. Comparing this result with the result from unphosphorylated stathmin, it was concluded that phosphorylation is decreasing the affinity of the stathmin to the tubulin dimers and thus the effective concentration of tubulin dimers is higher, which results in higher effective tubulin concentration (Figure.2-4).

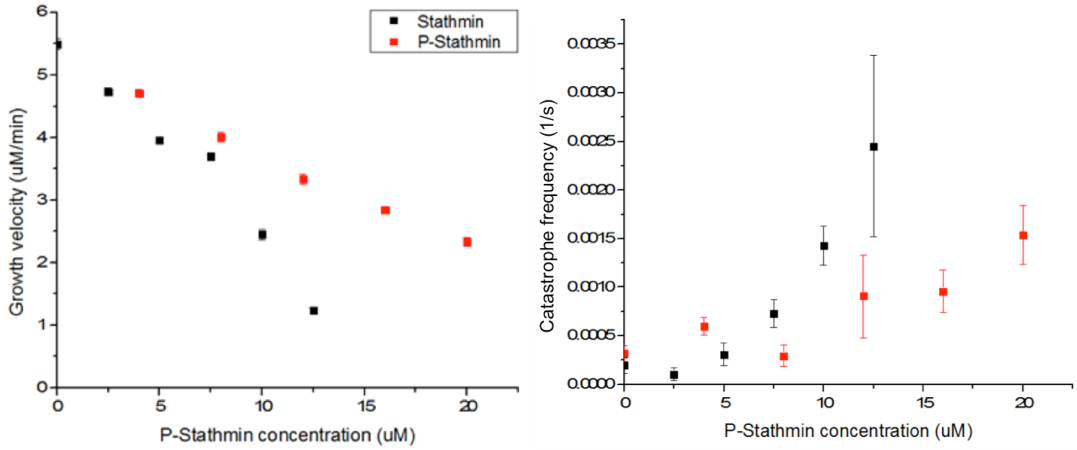

Figure.2-4 Stathmin phosphorylation affects its affinity to tubulin. Increasing phosphorylated stathmin at 40 μM tubulin decreases the growth velocity (left graph) and increases catastrophe frequency (right graph). But since the affinity of the stathmin to tubulin is decreased due to phosphorylation, at same concentration of stathmin, phosphorylated stathmin does not sequester tubulin efficiently (error bars correspond to S.E.M).

Inhibitory effect of the stathmin on microtubule dynamics is affected by its phosphorylation. In the cells, microtubule dynamics is locally regulated by a phosphorylated stathmin gradient, specially during mitosis (Niethammer et al., 2004, 2007). To measure microtubule dynamics in the presence of a phosphorylated stathmin gradient, different ratio of phosphorylated stathmin to unphosphorylated stathmin at constant total stathmin concentration, was introduced in the system. At lower phosphorylated stathmin fractions, no microtubule growth was observed. However, increasing the phosphorylated stathmin fraction increased the growth velocity. On the other hand, the catastrophe frequency was decreased. This observation suggests that as dynamic microtubules reach the phosphorylated stathmin gradient, microtubules are exposed to higher tubulin concentration, due to decreasing the affinity of phosphorylated stathmin to tubulin dimers, where microtubules grow faster, which leads to longer microtubules (Figure.2-5).

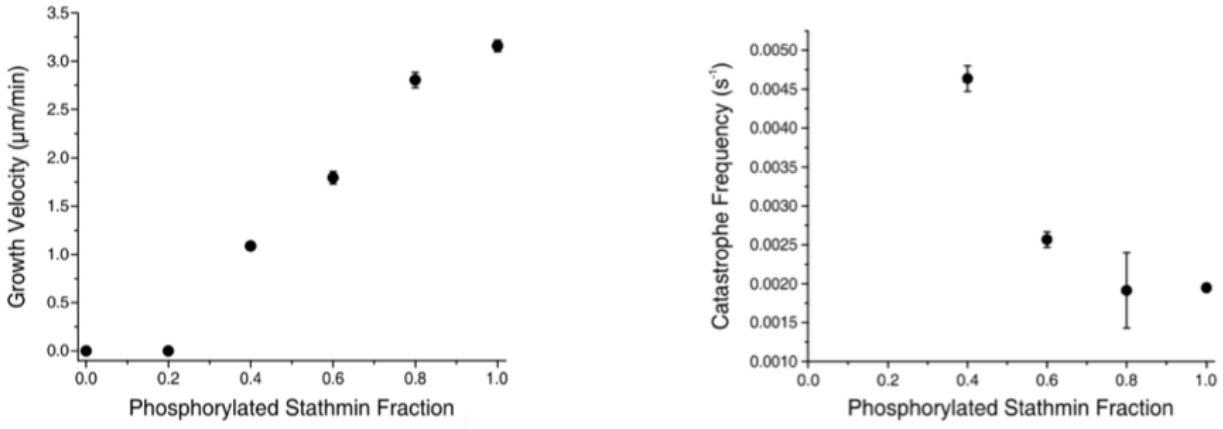

Figure.2-5 Effect of phosphorylated stathmin ratio on microtubule dynamics. Increasing the phosphorylated stathmin ration results in the increased growth velocity (left graph) and decreased catastrophe frequency (right graph) (error bars correspond to S.E.M).

4.2-The effect of tubulin concentration and stathmin phosphorylation on the size of microtubule asters

Microtubule dynamics is affected by the concentration of the tubulin and tubulin-sequestering agent, stathmin. Also, stathmin phosphorylation affects the microtubule dynamics. To investigate the effect of tubulin and stathmin, in phosphorylated and unphosphorylated state, on the microtubule asters, different experiments with purified centrosomes, as the organizing centers for dynamic microtubules, were designed.

The overall dynamics of microtubules affect the size of the microtubule aster. In order to measure the size of the microtubule asters, purified centrosomes were used as the microtubule-organizing center together with tubulin. The relative size of the aster (in the absence of confinement) was determined using confocal laser scanning microscopy (CLSM) and trace amounts of fluorescently labeled tubulin (10 % Alexa568- or Alexa488-tubulin). The fluorescence intensity decay of the microtubules from the center of the microtubule aster was measured to yield the size of the aster. Increasing the tubulin concentration resulted in the bigger microtubule asters. This result suggests that as microtubule asters are exposed to the higher tubulin concentration, microtubules grow faster and longer, as a result of decreasing the catastrophe frequency.

To study the effect of stathmin on the relative size of the microtubule aster, different concentrations of stathmin were introduced at high tubulin concentration. Stathmin decreases the effective concentration of tubulin dimers, and thus decreases the growth velocity and increases catastrophe frequency, which results in decreasing the size of the microtubule aster (Figure.2-6).

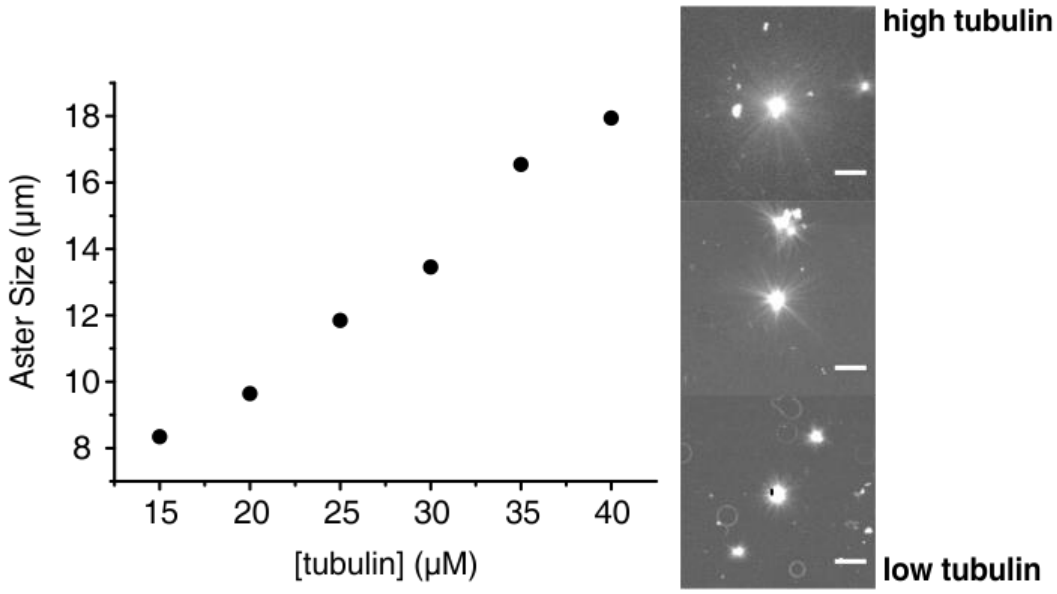

Figure.2-6 Size of microtubule asters is affected by tubulin concentration. Increasing the tubulin concentration increases the size of microtubule asters in a linear manner.

However, in the same set of experiments with phosphorylated stathmin, the size of microtubule asters was affected differently. Phosphorylation of stathmin decreases its affinity to tubulin dimer, and as a result increases the effective tubulin concentration. This results in bigger microtubule asters at the same concentration of unphosphorylated stathmin (Figure.2-7).

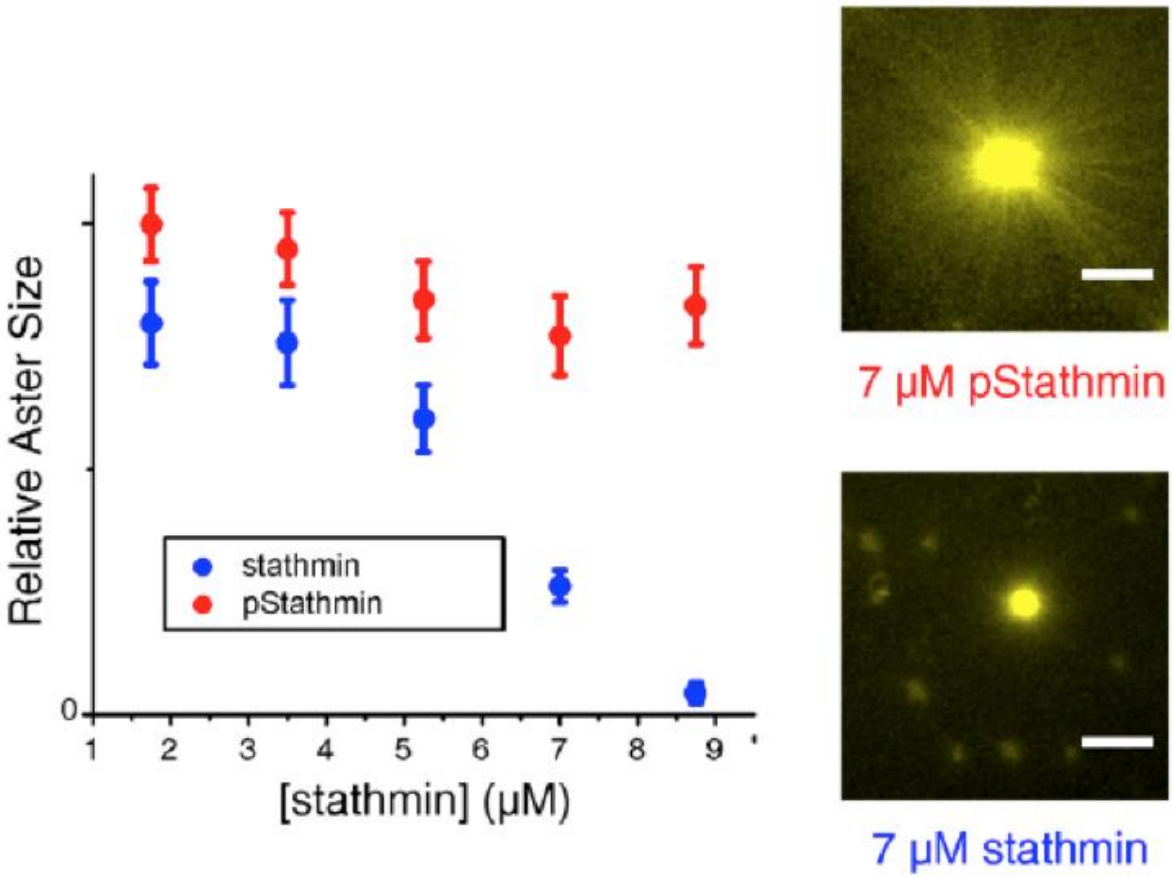

Figure.2-7 Size of microtubule asters is affected by stathmin phosphorylation.

Phosphorylation of stathmin decreases its inhibitory effect on microtubule dynamics. Microtubule asters' size is increasing as the result of stathmin phosphorylation (error bars correspond to S.E.M).

4.3-Microtubule-asters reorganizing themselves in response to their dynamics in deformable confinement

In the absence of confinement, microtubules are organized in radial arrays in the presence of microtubule organizing centers. To investigate the effect of confinement, as well as tubulin and stathmin concentration on the microtubule dynamics and organizing of the microtubule asters, microtubule organizing centers were encapsulated in GUVs together with tubulin dimers, using cDICE , where the tension in the membrane can be controlled by the outside osmolarity. As a result of previous experiments, size of the encapsulated microtubule aster can be controlled by the tubulin concentration.

The GUVs with encapsulated dynamic microtubule asters were monitored by confocal laser scanning microscopy (CLSM) using trace amounts of fluorescently labeled tubulin (10 % Alexa568- or Alexa488-tubulin). GUVs with low encapsulated tubulin concentration (15-25 μM) resulted in the organizing center of the small microtubule aster positioned in the center of the GUV (Figure.2-8 left GUV). Increasing the tubulin concentration (35-40 μM) resulted in cortical microtubules where the organizing center was positioned towards the membrane. However, decreasing the membrane tension by increasing outside osmolarity resulted in the formation of protrusions, affecting both position of the organizing center as well as overall morphology of the GUV (Figure.2-8 three right GUVs).

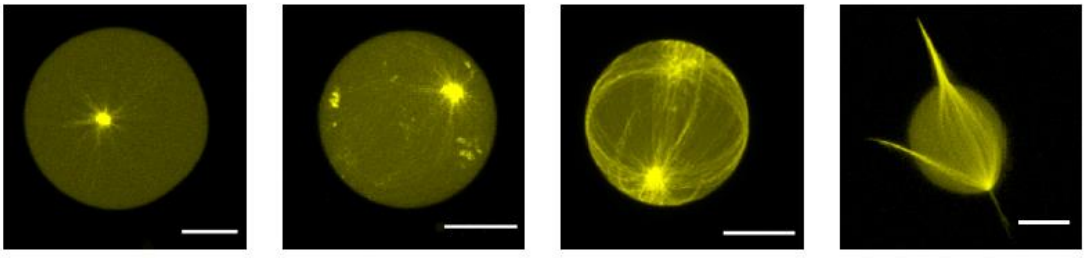

Figure.2-8 Effect of confinement on microtubule asters. At low tubulin concentrations, organizing centers are positioned in the center of the GUV (left GUV) while increasing tubulin concentration displaces the organizing center towards the membrane and changes the morphology to cortical (two middle GUVs) and even formation of protrusions, (polar morphology, right GUV). Scale bar = 10 μm

To investigate the formation and the dynamics of these microtubule-based protrusions, microtubule polymerization at high tubulin concentration was induced by raising the temperature from 20 °C to 34 °C, in GUVs with a rigid or deformable membrane. In the case of rigid membrane, increasing the temperature resulted in the decentering of the organizing center and formation of cortical microtubule aster (Figure.2-9 A). The kymograph of local membrane curvature shows that there was no deformation on the membrane due to high membrane tension. The position of the organizing center is shown with size of the black circles in the kymographs (large circle – peripheral organizing center). As the microtubule aster grows inside the GUV, the interaction between the microtubule aster and the membrane pushed the organizing center towards the membrane (Figure.2-9 B). Additionally, the overall shape and the position of the organizing center is shown the Figure.2-9 C.

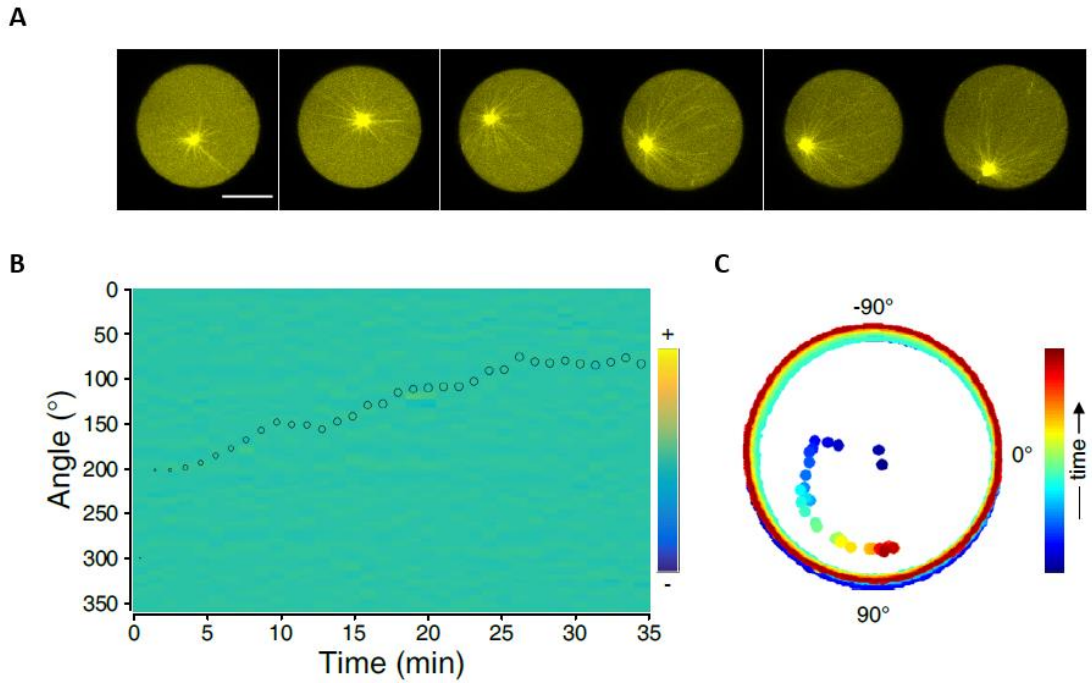

Figure.2-9 Growing Microtubule aster inside GUV. (A) The high membrane tension interacts with the growing microtubule aster and decenters the organizing center. **(B and C)** The kymograph of local membrane curvature shows no deformation on the membrane, but only decentering of the organizing center. Scale bar = 10 µm

However, upon growth of the microtubule aster in GUV with deformable membrane, the randomly distributed protrusions resulted in a stable morphology

with one or more protrusions in the main axes of the GUV, and the organizing center was positioned towards the membrane (Figure.2-10 A). In this case, initially growing bundles of the microtubule aster interact with the membrane and decenter the organizing center, which polarizes the microtubule aster and the protrusions. Upon decentering of the organizing center, more microtubules are growing towards the pre-existed microtubule bundles, as it is shown with the kymograph, which resulted in the deformation of the membrane (Figure.2-10 B). This recursive interaction between microtubule bundles and deformable membrane causes the stable polar morphology as described above.

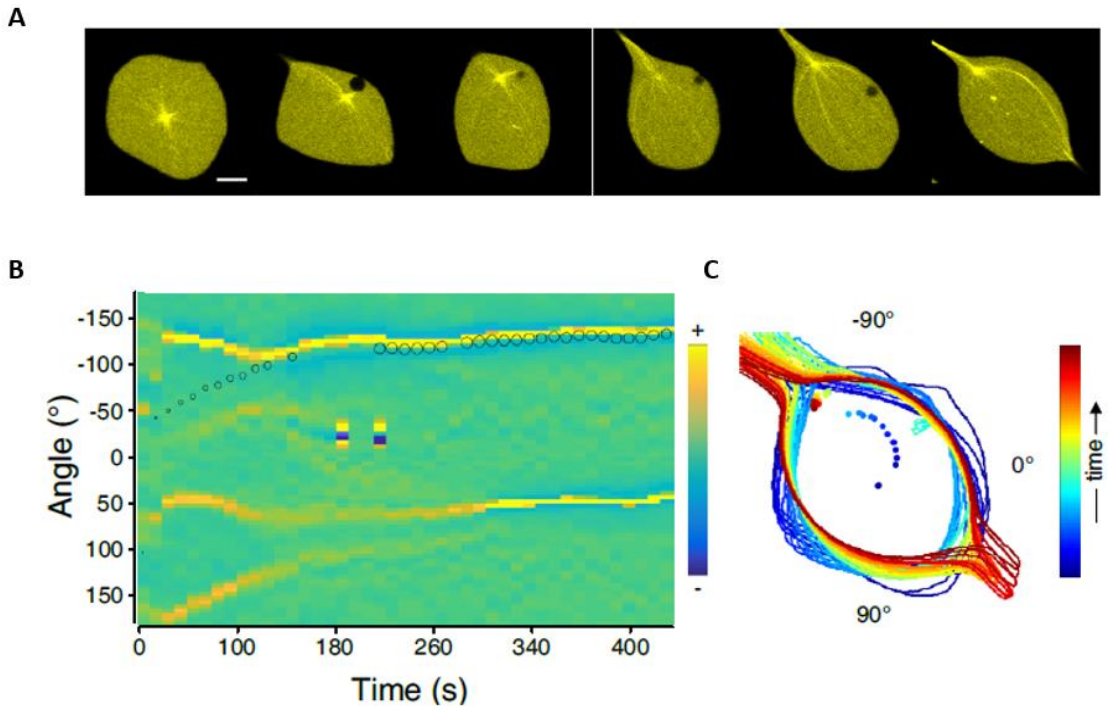

Figure.2-10 Growing microtubule aster in a deformable GUV. (A) Random protrusions because of interaction between microtubules and membrane result in the formation of a polar morphology. **(B and C)**. The local curvature shows that the randomly distributed microtubule-based protrusions interact with each other and form a more stable protrusion. This also affects the position of the organizing center. Scale bar = 10 µm

To investigate the global effect of stathmin and its phosphorylation on the size of the microtubule aster and the position of the organizing center, different

concentrations of stathmin were encapsulated together with microtubule asters in GUVs. Initially at high tubulin concentration, the organizing centers were positioned towards the membrane (Figure.2-11 A Black squares). The values close to 1 means the organizing center is positioned close to membrane. By increasing the concentration of stathmin, the organizing centers were re-centered which was caused by decreasing the effective concentration of tubulin dimer due to sequestering activity of the unphosphorylated stathmin. No protrusions were observed in this case (Figure.2-11 – Red squares). However, by encapsulating the same concentration of phosphorylated stathmin, the organizing centers were decentered again and positioned towards the periphery (Figure.2-11 A Blue squares). This is the result of decreasing the affinity of stathmin to tubulin dimer due to its phosphorylation and increasing the effective tubulin concentration. The formation of protrusions depends on the encapsulated concentration of tubulin and stathmin, as well as on membrane tension.

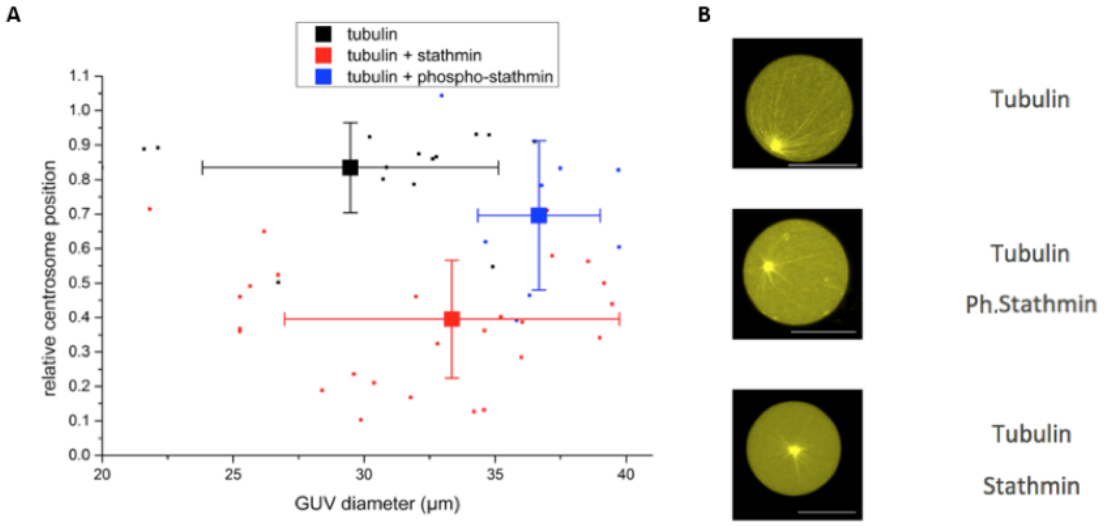

Figure.2-11 Effect of stathmin and its phosphorylation on the positioning of organizing centers. (A) Initially at higher tubulin concentration, the organizing centers are positioned towards the membrane (black squares). Introducing stathmin re-centers the organizing centers (red squares). **(B)** Stathmin phosphorylation decenters the organizing center again (blue squares). Examples of microtubule asters in GUV with high tubulin concentration (top), introducing stathmin (middle) and phosphorylated stathmin (bottom). Scale bar = 10 µm

4.4-recursive interaction between cytoskeleton and signaling gradient in deformable membrane: Synthetic Morphogenic Membrane System (SynMMS)

To investigate the response of the cytoskeleton to the stathmin phosphorylation gradient in confinement, a synthetic signaling system was encapsulated together with purified centrosomes and tubulin.

The signaling system consists of the previously developed iLID/SspB optical dimerizer system (Guntas et al., 2015), which was adapted in the Bastiaens lab to translocate SspB-AuroraB kinase to synthetic membrane bilayers via iLID, which is associated with the membrane using a C2 phosphatidylserine-binding domain (C2-iLID). This signaling system phosphorylates the microtubule regulator stathmin at the membrane. Stathmin is dephosphorylated in the cytosolic space of the GUV, where λ-phosphatase is present. This results in a phosphorylated stathmin gradient. This gradient provides a pool of high tubulin concentration at the membrane, which alters the microtubule dynamics.

The signaling system was encapsulated together with the dynamic microtubule aster (The full system is called Synthetic Morphogenic Membrane system – SynMMS).

First, upon investigation of the morphological distribution of non-activated SynMMS, it was observed that the morphologies that already existed with the encapsulated microtubule asters in absence of the signaling system, also occurred in this system as well (semi-aster: the spherical morphology where the organizing center is positioned towards the membrane; polar: where microtubule-based protrusions exist along the main axis of the GUV and the organizing center is positioned towards the membrane). However, anew morphology emerged. In this morphology, several microtubule-based protrusions are formed but not necessarily on the main axis of the deformed GUV. This new morphology is called star-like morphology (Figure.2-12).

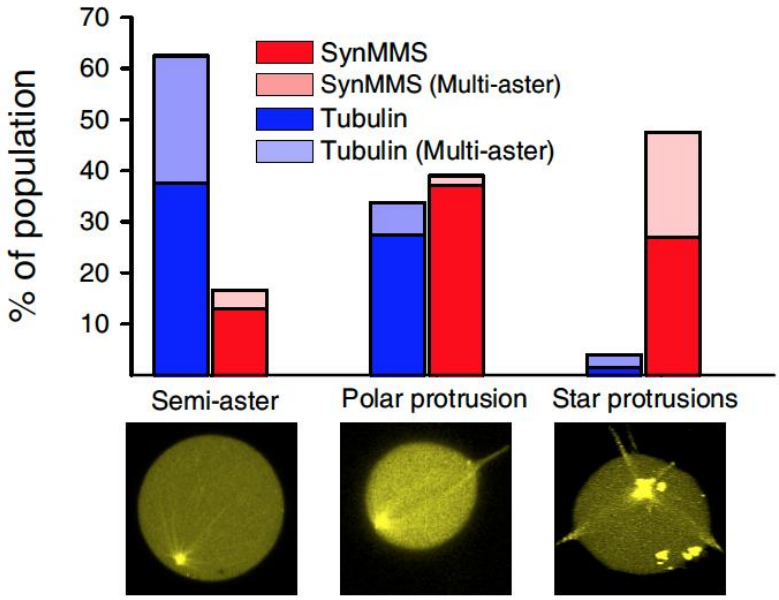

Figure.2-12 Morphological distribution of encapsulated microtubule asters and SynMMS. Encapsulated microtubule asters have two major morphologies, semi-aster and polar (Blue), while SynMMS forms a new star-like morphology (Red). The examples for each category are selected from the SynMMS system. The dim colors correspond to the GUVs with more than one microtubule aster.

Next, a SynMMS was subjected to global activation of signaling by continuously irradiating the whole GUV with blue light. Global activation of a spherical SynMMS with a small microtubule aster with a rigid membrane, led to kinase translocation and decentering of the organizing center (Figure.2-13) due to promoting the growth of the microtubule aster. Upon activation of the signaling system, the small microtubule aster interacts with the signaling system and growing microtubules apply a pushing force on the membrane which leads to the decentering of the organizing center. After activation, blue light was switched off and the organizing center responded by re-centering itself (Figure.2-12 top row). The contour plot corresponding to the time-lapse shows the decentering and re-centering of the organization center due to activation and relaxation, respectively (Fogure2-13 bottom row).

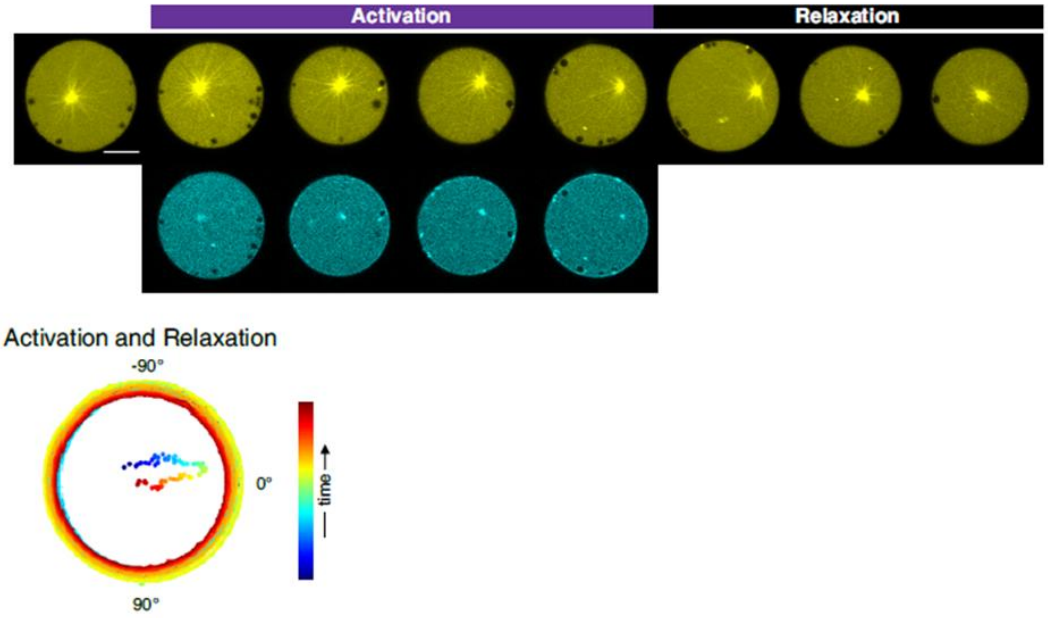

Figure.2-13 Response of SynMMS with rigid membrane and a small microtubule aster to global activation. Upon activation of the SynMMS, the organizing center is decentered due to the growing microtubule aster. This response was reversed during relaxation as the organizing center re-centered again. Yellow channel is tubulin and Cyan channel is Alexa488-SspB-AuroraB. Scale bar = 10 μm

To show that stathmin is the key component in the system which links cytoskeleton to the signaling system, a similar experiment was done without stathmin (SynMMS^{-stat}). SynMMS^{-stat} did not result in position change of the organizing center. This result proves that stathmin is the key to connect the signaling system to the cytoskeleton (Figure.2-14). The contour plot of the SynMMS^{-stat} shows that the position of the organization center does not change during the activation of the signaling system (Figure.2-14 bottom row).

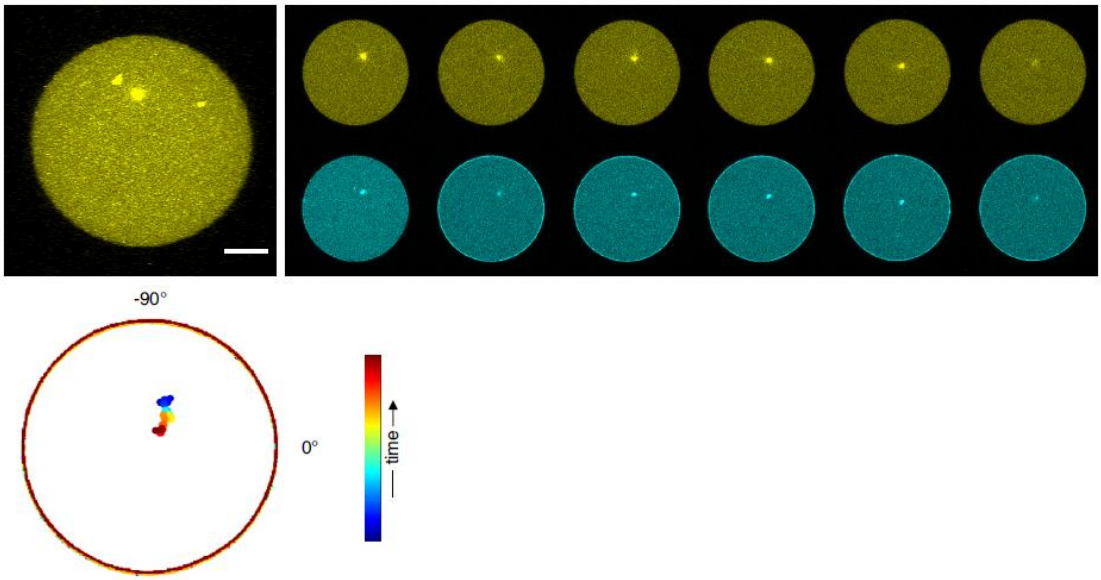

Figure.2-14 SynMMS^{-Stat} does not respond to activation of the signaling system. Upon activation of the signaling system, the position of the organizing center does not change due to the lack of stathmin in the signaling system. Yellow channel is tubulin and Cyan channel is Alexa488-SspB-AuroraB. Scale bar = 10 μm

To further study the recursive interaction between dynamic microtubule asters and the signaling system, SynMMS with the organizing center positioned towards the membrane in a GUV with reduced membrane tension was locally activated. This resulted in the immediate formation of a stable microtubule-induced protrusion in the activated region. Changing the activation region to the other side of the SynMMS also resulted in a stable microtubule-induced protrusion. However, upon third activation on a new region of the SynMMS, no protrusion was formed which indicates the depletion of microtubules into the two formed protrusions (Figure.2-15 A). The kymograph of local membrane curvature shows the persistence of the newly formed membrane deformation (Figure.2-15 B). Additionally, the persistence of the protrusions caused by previously locally activated regions, demonstrates that SynMMS possesses morphological memory (Figure.2-15 C).

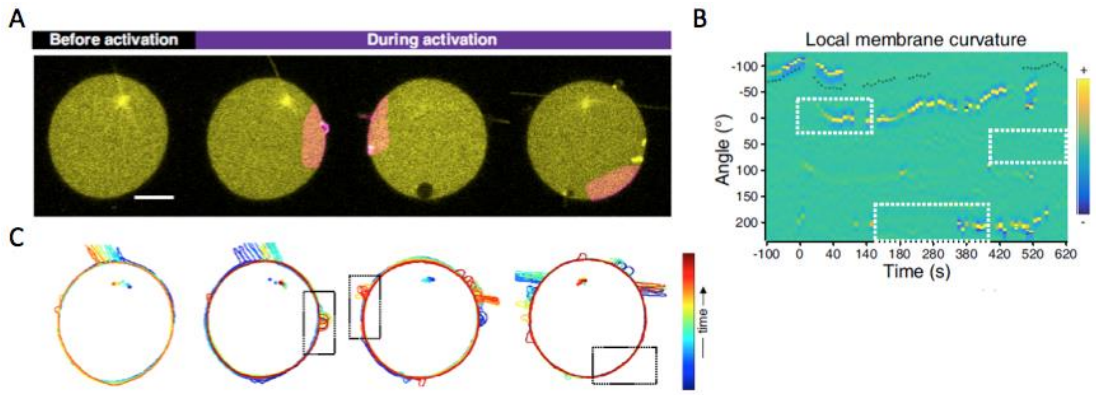

Figure.2-15 Local activation of SynMMS. (A) During local activation of SynMMS, newly formed membrane deformations are clearly connected to the microtubule aster. Upon changing the side of the activation, new deformations are formed in the activated region. But due to depletion of the kinase and microtubules during the first and second activations, there was no response to the third activation. **(B and C)** The kymograph of local membrane curvature as well as the contour of the activation series shows the persistence of these membrane deformations. The dashed lines mark the activation regions. Yellow channel is tubulin and magenta channel is Alexa488-SspB-AuroraB. Scale bar = 10 µm.

Next, to investigate the effect of initial morphological states on the response and post-activation morphology of the SynMMS, both SynMMS with a polar protrusion as well as a star-like morphology were activated globally with blue-light in increasing dose steps. In the polar morphology, SspB-AuroraB was recruited at the membrane protrusion already at low light-doses. This can be due to the high membrane surface to cytoplasmic volume ratio in the concave membrane protrusions (Rangamani et al., 2013; Schmick and Bastiaens, 2014) which increases SspB-AuroraB density on the membrane and enhances the phosphorylate stathmin gradient and leads to local activity of kinase in the protrusion (Figure.2-16 A). As a result, the pre-formed polar protrusions are stabilized. This suggests, SynMMS that have polar morphology with pre-formed microtubule-based protrusions will less likely to response to activation with global morphology changes. The position of the organizing center as well as the protrusion in the main axis of the deformed confinement is stabilized (Figure.2-16 B and C).

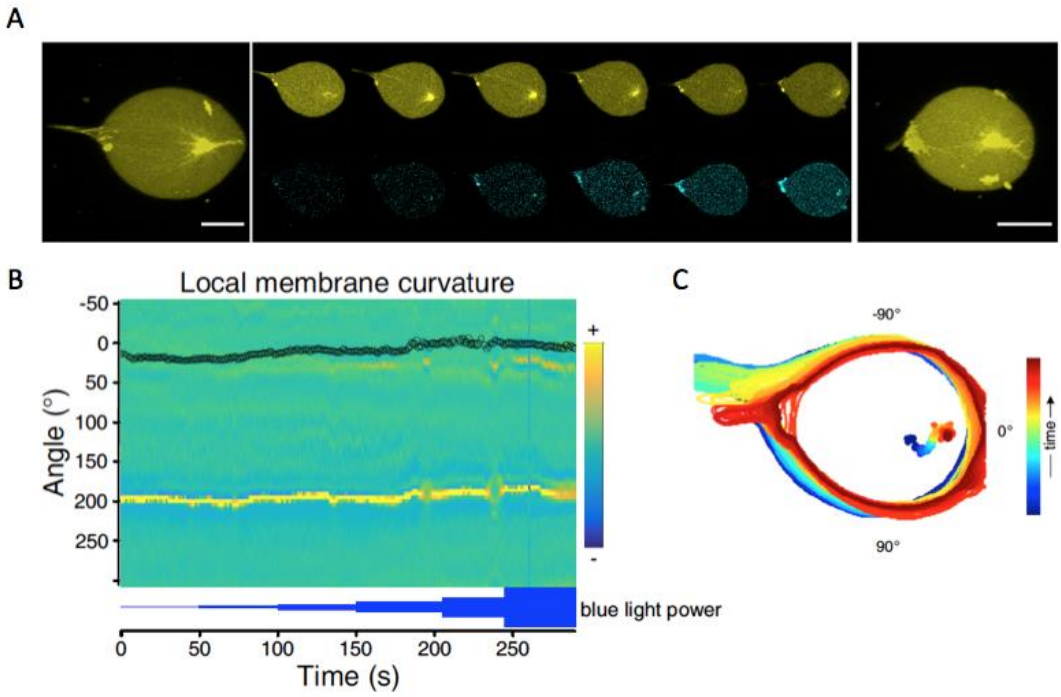

Figure2-16. Light-dose response of the polar SynMMS. (A) The signaling system is gradually activated in a SynMMS with a polar morphology. The first and last panels are corresponding to the morphology of the SynMMS before (left) and after (right) activation of the signaling system. **(B)** The position of the organizing center (the size of the black circles in the local membrane curvature) as well as the microtubule-based protrusion does not change after activation. **(C)** The contour of the SynMMS during activation shows that the microtubule-based protrusion was enhanced due to the dimensionality reduction mechanism of the curved membrane (Rangamani et al., 2013; Schmick and Bastiaens, 2014) but this does not affect the positioning of the organizing center. Yellow channel is tubulin and cyan channel is Alexa488-SspB-AuroraB. Scale bar = 10 µm.

On the other hand, global activation in different dose steps in the SynMMS with the initial star-like morphology resulted in decentering of the organizing center and a morphology change to a spherical shape. The pre-formed protrusions were stable in this case as well (Figure.2-17 A). This result again shows that enhanced signaling due to the pre-formed protrusions stabilized the microtubule-based protrusions (Figure.2-17 B). However, the growing microtubule aster responded to the activated signaling by changing the position of the organizing center (Figure.2-17 C).

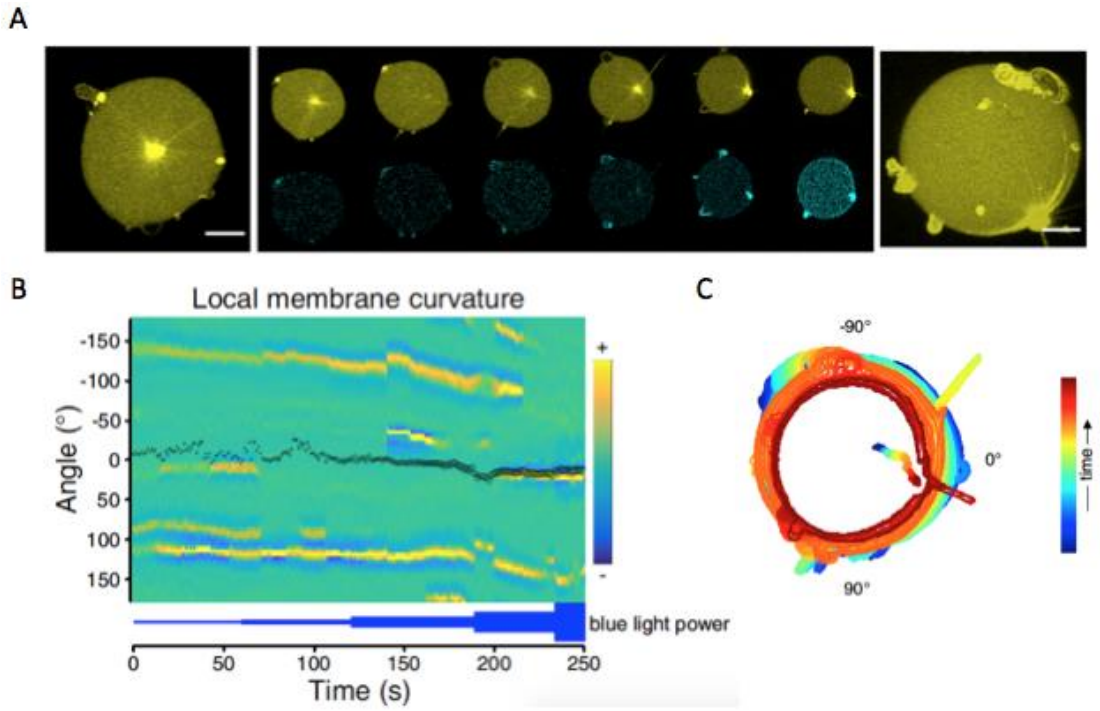

Figure2-17. Light-dose response of the star-like SynMMS. (A) The signaling system is gradually activated in a SynMMS. With a star-like morphology, which responded with changing the morphology to spherical. The first and last panels are corresponding to the morphology of the SynMMS before (left) and after (right) activation of the signaling system. **(B)** The position of the organizing center (the size of the black circles in the local membrane curvature) changes after activation. However, the microtubule-based protrusions are stabilized **(C)** The contour of the SynMMS during activation shows that the organizing center was positioned towards the membrane during the activation of the signaling system. Yellow channel is tubulin and cyan channel is Alexa488-SspB-AuroraB. Scale bar = 10 µm.

Furthermore, to study how a local activation of the signaling system changes the morphology of a SynMMS, a star-like SynMMS with the organizing center positioned in the center of the GUV was activated locally on the site between two major protrusions (Figure.2-18 A). The kinase translocation enhanced microtubule growth, which directed the pre-formed protrusion into the activated region. By further growth of the microtubules and due to the angle of the microtubule bundles with the membrane, microtubules were directed to the second pre-formed microtubule-based protrusion (Figure.2-18 A and B). This resulted in further stabilization of the second protrusion by directing the microtubule bundles that formed the lower protrusion. The contour of the SynMMS shows that the position of the organizing center is stable.

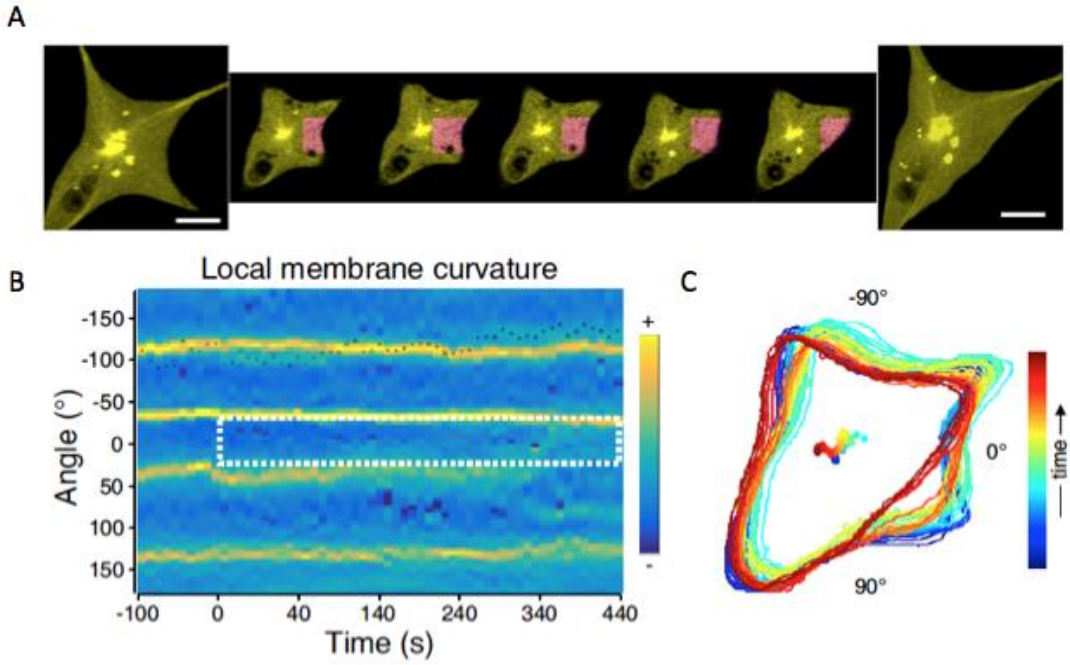

Figure2-18. Global activation of star-like SynMMs. (A) The signaling system is locally activated in a SynMMS with a star-like morphology responded with stabilizing the morphology. The first and last panels are corresponding to the morphology of the SynMMS before (left) and after (right) activation of the signaling system. **(B)** The position of the organizing center (the size of the black circles in the local membrane curvature) does not change after activation. **(C)** The contour of the SynMMS during activation shows that the organizing center was positioned towards the membrane during the activation of the signaling system. Yellow channel is tubulin and magenta channel is Alexa488-SspB-AuroraB. Scale bar = 10 μm.

5-Disscussion

In animal cells, the overall shape of the cell is tightly linked to the cytoskeletal network, especially to the dynamic microtubules that organized by microtubule organizing center, centrosome. These filaments are highly dynamic that continuously altering between polymerizing and depolymerizing phases (Mitchison and Kirschner, 1984). The microtubule dynamics is regulated by tubulin dimer concentration. Increasing tubulin concentration, promotes the growth velocity in a linear manner. In the higher tubulin concentrations, they are less likely to undergo catastrophe (Figure.2-2).

Stathmin is known to inhibit microtubule polymerization. Introducing stathmin into the system with high tubulin concentrations, acts as a tubulin-sequestering agent. This results to the slower growth of the microtubules (Figure.2-3). The inhibitory effect of the stathmin on microtubule dynamics is regulated by its phosphorylation (Niethammer et al., 2004). Stathmin phosphorylation increases the growth velocity of the microtubules, as stathmin's affinity to the tubulin dimers are decreased due to the phosphorylation.

Investigating the effect of tubulin concentration on the size of the microtubule aster polymerized from purified centrosomes shows that at higher tubulin concentrations, microtubule asters are more likely to grow (Figure.2-6). Introducing stathmin results the smaller asters at high tubulin concentration due to sequestering the tubulin dimers. Upon phosphorylation of the stathmin, due to higher effective tubulin concentration, the size of the microtubule asters increases (Figure.2-7).

Microtubules are responding to the regulating signals and the membrane of the cell, changing the shape of the membrane. The polarity resulted from the interaction between microtubules and motor proteins has been the subject of many studies (Baumann and Surrey, 2014, Juniper et al., 2018, Laan et al., 2012, Letort et al., 2016, Nédélec et al., 1997, Pinot et al., 2009, Surrey et al., 2001), however the question that how cell shape is resulted during recursive interaction between signaling at the membrane and dynamic cytoskeleton has not been answered yet.

For the encapsulated dynamic microtubule aster, membrane deformability promotes the formation of the microtubule-based protrusions (Liu et al., 2008; Schmick and

Bastiaens, 2014) that directly guides microtubules into the formed protrusion and thus changes the morphology.

The basic concept of local matter coalescence through self-amplification, which in turn depletes the substrate from the surrounding represents a minimal model through which stigmergy can be realized, and can therefore exemplify a large class of systems (Deneubourg, 1977; Susnea and Axenie, 2015; Tabony, 2006; Theraulaz et al., 2003). Bringing it to the molecular systems relevant to SynMMS, the concept of the self-induced capture sites of membrane protrusions (Schmick and Bastiaens, 2014) is stigmergic. The microtubule-based protrusions resulting from the interactions of the dynamic microtubule aster with the deformable membrane will capture more microtubules polymerized from organizing center, thus generating self-induced capture sites that deplete radially distributed microtubules.

The encapsulated fuel in the form of ATP and GTP established the non-equilibrium conditions, is essential for self-organized morphological states of SynMMS. The recursive interaction between microtubule dynamics, morphology of the SynMMS, and signaling resulted in SynMMS morphogenic responses, where The SynMMS not only responses to the regulating signal, but for the ensuing response that is shaped by the internal state resulting from prior morphological state. The light-induced transitions between morphological states are thereby triggered by changes of the substrate bifurcation parameter in the signaling module.

To study the effect of the confinement, dynamic microtubule asters were encapsulated in GUVs. The size of the aster effects the position of the organizing center. Bigger microtubule asters are positioning their organizing center towards the membrane. This causes the formation of the cortical microtubules (semi-aster morphology) in the rigid membrane (Figure.2-8). This rigidity is linked with the tension in the membrane, which can be regulated with changing the osmolarity of the outside solution. With deformable membranes, when the organizing center is pushed towards the membrane, microtubule bundles are forming and these bundles are more likely to originate microtubule-based protrusions. These protrusions are positioned along the main axis of the deformed GUV (polar morphology) (Figure.2-8). The dynamics of the formation of these protrusions suggest that upon growth of the microtubule aster, randomly distributed microtubule bundles are interacting with the deformable

membrane and forming several protrusions (Figure.2-10). As the microtubule aster is becoming larger than the size of the confinement, applied force due to the interaction between the microtubule bundles and membrane, forces these protrusions to coalescence into one or two protrusions, and changes the position of the organizing center towards the membrane (Figure.2-10). Introducing the stathmin and phosphorylated stathmin, re-centers and decenters the organizing center (Figure.2-11)

Integrating the encapsulated microtubule aster with a signaling system, which translocates the kinase to the membrane via an optical dimerizer, results a new morphology.

The star-like morphology, where the organizing center is not positioned at the membrane and several microtubule-based protrusions are formed, suggests that the signaling system is stabilizing the protrusions via enhancing the phosphorylated stathmin in the deformed membrane where the ratio of the membrane surface to the cytoplasmic volume is higher (Rangamani et al., 2013, Schmick and Bastiaens, 2014). In SynMMS, Stathmin is the key to link the microtubule aster to the signaling system (Figure.2-14). Global activation of a SynMMS with rigid membrane and an organizing center positioned in the center of the confinement, positions the organizing center towards the membrane, and the organizing center re-centeres again during relaxation (Figure.213). Local activation of a SynMMS results in the formation of new protrusions as well as decentering the organizing center in the case of a polar and star-like morphologies (Figure.2-15). These protrusions are stable and remain even after relaxation.

On the other hand, local activation of a SynMMS with a star-like morphology with strong microtubule-based protrusions results in coalescence of the protrusions into a one stable protrusion (Figure.2-18).

Much has to be learned from SynMMS on the structural stability of the emergent morphological states that are a direct consequence of the attractors of the system, as well as on its plasticity and reversibility in response to external stimuli. For example, since membrane deformation by MT-bundles actuate signaling, we also expect that morphological state transitions in SynMPS can be triggered by externally imposed mechanical stimuli that deform the membrane.

6-Materials and Methods

6.1-Preparation and labeling of tubulin

Tubulin purification was performed according to a standard method (Castoldi and Popov, 2003). The following deviations from the published procedure were made:

20 fresh pig brains (40 halves) were transported from the slaughterhouse in ice-cold PBS buffer (NaCl 137 mM, KCl 2.7 mM, Na_2HPO_4 10 mM, KH_2PO_4 1.8 mM, pH 7.4). After transportation, brains were removed from the PBS buffer, and the meninges and the brain stem were removed using paper towels. Peeled brain was mixed with depolymerization buffer (DP) (in the ratio of buffer volume/brain mass 1.5 l/kg - MES 50 mM, $CaCl_2$ 1 mM, pH 6.6 NaOH). 1 mL of PMSF (1 M) was added to the mixture. The mix was homogenized in the blender (1 min at low speed, 1 min rest, two times of 1 min at high speed with 2 min rest time in between). The pH of the homogenate was set to 6.8 using KOH. After that, the homogenate was filled into SLA-1500 and F14 (Thermo Scientific) buckets (250 mL Nalgene). The homogenate was spun down at 14000 rpm at 4 ºC for 60 min.

The pre-warmed (37 ºC) High Molarity PIPES Buffer (HMPB) (PIPES 555 mM, $MgCl_2$ 5.5 mM, EGTA 11.1 mM, Glycerol 55% vol., pH 6.9 KOH), ATP (200 mM) and GTP (200 mM) was added to the supernatant to the final concentration of 333 mM, 1.5 mM and 0.5 mM respectively. The temperature was raised rapidly to 37 ºC in the water bath (50 ºC) and when the mix reached the temperature; it was transferred to the water bath at 37 ºC and incubated for 90 min (stirred regularly). PIPES powder was used to adjust the pH to 6.8 when necessary. The pre-warmed Ti-45 rotor (Beckman Coulter) was used to spin down the mix at 42000 rpm for 30 min at 37 ºC.

The pellet in each tube was suspended in 2 mL of cold DP buffer on ice. The mix was kept on ice and forced to depolymerize by pipetting up and down. After depolymerization, the mix was spun down in a Ti-45 rotor at 35000 rpm for 30 min at 4 ºC.

The supernatant was carefully decanted into a graduated cylinder. Pre-warmed HMPB, ATP and GTP were added to the supernatant to the final concentration of 333 mM, 1.5 mM and 1 mM respectively. The temperature was rapidly raised to 37 ºC using the water bath at 50 ºC. After reaching 37 ºC, the mix was transferred to the water bath at 37 ºC and incubated for 30 min. Then the supernatant was spun down in Ti-45 rotor at 42000 rpm for 30 min at 37 ºC.

The supernatant was carefully and completely discarded and the pellet was resuspended in 25 mL of cold BRB80 (PIPES 80 mM, $MgCl_2$ 1 mM, EGTA 1 mM, pH 6.8 with KOH). The mix was depolymerized on ice. The mix was spun down in a P28-S rotor (Hitachi) at 24000 rpm for 20 min at 4 ºC. The supernatant was removed carefully and the concentration was measured and adjusted to 200 µM with BRB80.

Aliquots of 100 µL (50 µl is more practical for SynMMS experiments) were frozen in liquid nitrogen. 500 µl aliquots are advisable for future labeling.

Tubulin was labeled with NHS-Alexa488, -568 or -647 (Thermo Fisher Scientific) or EZ-link NHS-biotin (Thermo Fisher Scientific) according to a standard procedure (Hyman et al., 1991).

52.3 mg of 200 µM tubulin was thawed. $MgCl_2$ and GTP were added on ice to the final concentration of 2.5 and 1 mM respectively. Half the volume of pre-warmed (37 ºC) glycerol was added to the mix and the mix was incubated in a water bath (37 ºC) for 30 min. The polymerized tubulin was added on top of 2.5 mL pre-warmed High pH cushion (HEPES 100 mM, $MgCl_2$ 1 mM, EGTA 1 mM, Glycerol 60% vol., GTP 0.5 mM, pH 8.6 with KOH before adding glycerol). The mix was spun down in an MLA-80 rotor (Beckman Coulter) at 75900 rpm for 45 min at 37 ºC. The supernatant was removed carefully and the interface was washed two times with 1 mL of pre-warmed labeling buffer (HEPES 100 mM, $MgCl_2$ 1 mM, EGTA 1 mM, Glycerol 640% vol., GTP 0.5 mM, pH 8.6 with KOH before adding glycerol). Then, the cushion was removed carefully and the pellet was resuspended with 1 mL of cold labeling buffer with a cut-off 1 mL pipette tip until no tubulin chunks were visible.

2.5 mg of NHS-ester (Succinimidyl Ester) dye was dissolved in 32 µL DMSO. Half of the volume of the dye was added to the mix and gently mixed every 5 minutes in the water bath (37 ºC). After 15 min, the second half was added to the mix and the mix was gently mixed every 5 min for 10 min. The mix was then added on top of 4 mL of pre-warmed low pH cushion (BRB80 1x (from 5x stock – PIPES 400 mM, $MgCl_2$ 5 mM, EGTA 1 mM, pH 6.8 with KOH), Glycerol 60% vol., pH 6.8 with KOH) and was spun down in an MLA-80 rotor at 75900 rpm for 25 min at 37 ºC.

The supernatant was removed carefully and the interface was rinsed two times with 1 mL of pre-warmed 1x BRB80. Then, the cushion was removed carefully and the pellet was resuspended on ice in 0.6 mL of ice-cold injection buffer (K-Glutamate 100 mM, GTP 1 mM $MgCl_2$ 1 mM, pH 7). The mix was incubated on ice for 20 min. After

that, the mix was spun down in an RP45A rotor (Sorvall Centrifuge) at 45000 rpm for 10 min at 2 ºC.

The supernatant was recovered, and BRB80, $MgCl_2$ and GTP were added to the mix to the final concentration of 1x, 2.5 mM and 1 mM, respectively. The mix was incubated on ice for 3 min and then, pre-warmed glycerol was added to the mix to the final concentration of 33% vol. and the mix was transferred to 37 ºC and incubated for polymerization for 30 min. The mix was spun down on top of 4 mL of pre-warmed low pH cushion in an MLA-80 rotor at 75900 rpm for 25 min at 37 ºC.

The supernatant was removed and the cushion was rinsed two times with 0.5 mL of pre-warmed BRB80. The cushion was carefully and completely removed and the pellet was resuspended completely in 0.4 mL of cold BRB80 using a cut-off pipette tip. The mix was incubated on ice for 20 to 30 min. The mix was finally spun down in an RP45A rotor at 45000 rpm for 10 min at 2 ºC. At the end the concentration was adjusted to 200 µM using cold BRB80 and the tubulin was frozen and stored at -150 ºC in 5 or 10 µl aliquots.

6.2-Preparation of centrosomes

Centrosomes were isolated from KE37 cells following a standard method (Bornens and Moudjou, 1999).

2.8 L of suspension KE37 cells at the density of $1.3x10^6$ (cell/mL) were used to purify centrosomes. Nocodazole (0.33 M) and cytochalasin D (1 µg/mL in DMSO) were added to the cells at a final concentration of 16.5 mM and 5 mg/mL, respectively and incubated for 1 hour at 37 ºC. The cells were spun down in an F10-6x500y rotor (500 mL buckets – Thermo Scientific) at 2100 rpm for 5 min at 4 ºC. The pellet was then resuspended in 1.4 L of TBS buffer (from 10x TBS buffer - Tris 200 mM, NaCl 1.5 M, pH 7.4). The cells were spun down in an F10-6x500y rotor at 2100 rpm for 5 min at 4 ºC. The mix was resuspended in 0.7 L of TBS 1/10 – 8Suc. buffer (Tris 2 mM, NaCl 15 mM, Sucrose 8% vol., pH 7.4) and spun down in an SLA-1500 rotor (250 mL buckets - Thermo Scientific) at 2300 rpm for 5 min at 4 ºC.

The mix was resuspended in 20 mL of TBS 1/10 – 8Suc. buffer. The lysis buffer (HEPES 1 mM, NP40 0.5% vol., $MgCl_2$ 0.5 mM, β-mercaptoethanol 0.1% vol., leupeptin 1 µg/mL, pepstatin 1 µg/mL, aprotinin 1 µg/mL, PMSF 1 mM, pH 7.2) was added to adjust the final concentration of the cells to 10^7 (cell/mL) and the cells were resuspended with a 10 mL pipette for 5 min. The mix was spun down in an SLA-1500 rotor at 4100 rpm for 10 min at 4 ºC. The supernatant was filtered through a nylon mesh (53 µm mesh size), and PIPES (1 M) and DNase I (1 mg/mL) were added to the mix to a final concentration of 10 mM and 1 µg/mL, respectively, and the mix was incubated for 30 min at 4 ºC. The mix was then spun down on top of 8.6 mL of 60% Suc. cushion in a P28-S rotor (Hitachi) at 7400 rpm for 30 min at 4 ºC. The supernatant was removed until 25 mL of it was left. The mix was briefly resuspended and again spun down on top of step gradient sucrose cushions (4 mL of 70%, 2.5 mL of 50%, 2.5 mL of 40 % in each tube – total of 30.7 mL) in a P28-S rotor at 14900 rpm for 60 min at 4 ºC. The fractions of 0.5 mL were collected from the bottom of the tube. The simple polymerization assay in bulk with 40 µM tubulin in BRB80 was used to check which fractions had purified centrosomes. Aliquots of 10 µl were shock frozen and stored at -80 °C.

6.3-Protein encapsulation in GUVs by cDICE

Encapsulation of proteins in GUVs was achieved by continuous Droplet Interface Crossing Encapsulation following the original method (Abkarian et al., 2011) with relevant parameters noted below.

0.36 mM lipids were prepared in mineral oil (M3516, Sigma Aldrich/Merck, Darmstadt, Germany). The mixture consisted of eggPC (Sigma Aldrich/Merck) with 15 mol% DOPS and 0.05 mol% DOPE-biotin (both from Avanti Polar Lipids, Alabaster, U.S.A.). Additionally, 0.05 ml% LissamineRhodamineB-DOPE was added for experiments to image GUV membranes. Glass capillaries were typically 10 – 15 µm wide, and pressure was applied using an MFCS-EZ control system (Fluigent, Jena, Germany). cDICE chambers were 3.5 cm wide and were rotated at 1500 – 1800 rpm. 8-well Lab-Tek chambers (Thermo Fisher Scientific) or 18-well µ-slides (ibidi, Martinsried, Germany) were coated with streptavidin for GUV immobilization.

The base cDICE buffer contained 80 mM Pipes pH 6.8, 75 mM KCl, 2 mM $MgCl_2$, 1 mM EGTA, 1 mM trolox, 0.1 mg/ml β-casein. Additionally, the inner buffer contained 300 mM sucrose and 80 mM glucose, while the outer buffer contained 380 mM glucose. Whenever an osmotic deflation of GUVs to decrease membrane tension was desired, the sucrose concentration inside was lowered by 60 mM and the outside glucose concentration was increased by 160 mM. To induce deflation of GUVs, 50 µl of 1 M glucose were added to 300 µl of GUVs.

In experiments involving PPλ, EGTA was replaced by 0.8 mM $MnCl_2$. For tubulin polymerization, 2 mM GTP was included, whereas phosphorylation gradient experiments just required the presence of soluble tubulin, for which 60 µM GTP were included. For AuroraB, 2 mM ATP was added, and in experiments requiring both nucleotides the $MgCl_2$ concentration was increased to 4 mM. Oxygen scavengers were included in cases with just microtubule asters and stathmin, but were omitted in all other encapsulation experiments.

The encapsulation efficiency of tubulin and stathmin was determined by a reference concentration outside of GUVs, and the used protein concentration in cDICE was adjusted to yield desired final concentrations, as indicated in respective experiments. For encapsulation of centrosomes, the samples typically contained 10 vol% of a purified centrosome fraction.

For the encapsulation of iLID, AuroraB, and PPλ, an exact concentration was not targeted, but the resulting inside concentrations and membrane densities given specific starting concentrations were quantified and verified to result in sufficient membrane recruitment and desired stathmin phosphorylation state.

Prior to cDICE, the samples were centrifuged for 15 min at 100.000 rpm in a TLA-100 rotor (Beckman Coulter). The centrosomes were never centrifuged, while the tubulin stock was centrifuged separately for 30 min at 60.000 rpm in an RP80-AT2 rotor (Sorvall/Thermo Fisher Scientific).

6.4-Imaging of MT asters and morphological states in GUVs

To produce MT asters in GUVs, soluble tubulin and centrosomes were encapsulated as described. Stathmin was included as indicated for individual experiments. The following protein concentrations were used in the full reconstituted morphogenic system: 40 or 44 µM (final) tubulin (10 % Alexa647-tubulin), 4 µM (final) stathmin, 5 µM Gly-C2-iLID, 12 µM Alexa488-SspB-AuroraB/INCENP, 1 µM λ-PPase. Alexa568-tubulin was used for experiments without the signaling system at indicated concentrations.

Imaging was done on a Leica SP8 confocal microscope (Leica Microsystems, Wetzlar, Germany) equipped with Leica HyD hybrid detectors at 33 °C in an environment-controlled chamber (Life Imaging Services, Basel, Switzerland) using an HC PL APO 63x/1.2NA motCORR CS2 water objective (Leica Microsystems). The elevated temperature promoted tubulin polymerization, the asters reaching their end state in ca. 7 minutes, after which single-plane images or z-stacks (1 or 0.5 µm spacing) were taken. For the temperature ramp experiments, GUV-containing Lab-Tek chambers were incubated at 4 °C for 10 minutes in the pre-cooled Stable Z Lab-Tek Stage (Bioptechs, Butler, U.S.A.). Then, the stage was moved onto the microscope equilibrated at room temperature and reached RT (~ 21 °C) in 10 minutes. The measurements indicated as “cold” were done under this condition. After that the Stable Z Lab-Tek Stage controller was used to heat the sample to 34 °C within 20 minutes and images were taken every minute.

Alexa568 or Alexa488 were excited with a 470 – 670 nm white light laser (white light laser Kit WLL2, NKT Photonics, Köln, Germany) at 578 nm (270 – 600 mW/cm²)

or 488 nm (220 – 340 mW/cm²), respectively. Detection of fluorescence emission was done in standard or counting mode, restricted with an Acousto-Optical Beam Splitter (AOBS) to 588 – 640 nm or 498 – 540 nm, respectively. Images were taken with 2-4x line averaging at 400 or 200 Hz scanning speed. The pinhole was set to 1 Airy unit here and in all experiments described in this work.

In the full morphogenic system, Alexa647 was excited at 650 nm (200 mW/cm² - 700 mW/cm²) at 1000 Hz scanning speed to reduce photodamage. Detection of fluorescence emission was done in counting mode, restricted to 650 – 750 nm and further restricted by LightGate time-gating to minimize signal from laser reflection and background. Activation of iLID and imaging of Alexa488-SspB-AuroraB was done with 488 nm (220 mW/cm²) excitation from a white light laser source, restricting detection to 498 – 580 nm and by LightGate. Time series images and stacks (1 µm spacing) were taken with 8x line accumulation in line sequential scanning mode. For local activation, 488 nm illumination was restricted to a manually drawn ROI.

6.5-Single-filament TIRF-M assay and data analysis

GMPCPP-stabilized microtubule seeds were prepared as follows: 40 µL of 40 µM tubulin mixture (25 % tubulin, 25 % Alexa568-tubulin, 50 % biotinylated tubulin) was polymerized in seed buffer (80 mM Pipes pH 6.8, 1 mM $MgCl_2$, 1 mM EGTA, 1 mM GMPCPP (Jena Bioscience), 5 mM β-mercaptoethanol) at 37 °C. After 30 minutes, 400 µL of prewarmed BRB80 (80 mM Pipes pH 6.8, 1 mM $MgCl_2$, 1 mM EGTA) was added to the tubulin mixture, which was then spun down in a table top centrifuge at 21.000 g for 8 minutes at RT. The microtubule pellet was thoroughly resuspended in 40 µL of BRB80.

TIRF flow chambers were assembled from a biotin-PEG functionalized glass coverslip attached to a PLL-PEG passivated cover slide using double-sided tape (Bieling et al., 2010). To prevent potential unspecific binding, the flow chamber was first flushed and incubated with 35 µL of blocking buffer (100 β-casein µg/mL, 1 % w/v Pluronic F-127 in assay buffer (40 mM Pipes pH 6.8, 75 mM KCl, 4 mM $MgCl_2$, 0.4 mM EGTA, 1 mM GTP, 100 β-casein µg/mL, 1 mM trolox, 20 mM β-mercaptoethanol). After 5 minutes, the flow chamber was washed two times with 35 µL of assay buffer. Then, the chamber was flushed and incubated with 35 µL of 150 µg/mL Neutravidin (Thermo Fisher Scientific) in assay buffer for another 5 minutes. The flow chamber was washed two times with 35 µL of assay buffer, and then the chamber was flushed and incubated with 35 µL of diluted (1:750) GMPCPP-stabilized microtubule seeds. After 5 minutes, the chamber was washed two times with 35 µL of assay buffer.

After the seeds were immobilized on the surface, 40 µL of protein mixture (10 – 40 µM tubulin (7.5 % Alexa568-labeled), 0 – 20 µM stathmin, 0 – 30 µM phospho-stathmin, 4 µL 10x oxygen-scavenging system (Bieling et al., 2010), 0. 2% w/v methylcellulose) in assay buffer was introduced into the flow chamber and the two sides were sealed with transparent nail polish.

Imaging was performed at RT with a custom-built TIRF microscope (Olympus IX81 base) with a 60x Olympus APON TIRF objective with TOPTICA IBeam smart 560s laser and a Quad-Notch filter (400-410/488/561/631-640). Temperature was kept at 34 °C by a collar objective heater (Bioptechs). Image acquisition was done with an EM CCD Andor iXon 888 camera controlled by Micromanager 1.4 software. Fiji

ImageJ was used for data analysis. For each condition, the average growth velocity and catastrophe frequency were determined from ≥60 microtubules by kymograph analysis.

6.6-Determination of MT-aster size *in vitro*

20 µL of protein mixture (10 – 40 µM tubulin (7.5 % Alexa568-labeled), 0 – 20 mM stathmin, 0 – 30 µM phospho-stathmin, 2 µl Silica beads (SS06N, Bangs Laboratories, Fishers, U.S.A.), 2 µl 10x oxygen-scavenging system (Bieling et al., 2010), 0.2 % w/v methylcellulose) was dispersed on a glass cover slide blocked with PLL-PEG (Bieling et al., 2010) and covered with a glass coverslip pre-coated with PLL-PEG. The edges were sealed with transparent nail polish. Imaging of asters at 33 °C or in temperature ramp experiments were done as described in "Imaging of microtubule asters and morphogenic state transitions in GUVs". 12 µm thick z-stacks (1 µm spacing) were taken in the experiments at 33 °C, but single planes were taken during the temperature ramp to maximize the number of imaged fields of view.

For each individual condition, the z-stacks (if present) of each position were average projected in Z and aligned on each other, and projected again using a custom macro in ImageJ. The radial intensity profile of the averaged data (> 30 asters per condition) was extracted with a custom ImageJ macro. The aster size was determined as the 99 % decay length of a mono-exponential fit to the radial intensity profile in Origin (OriginLab, Northhampton, U.S.A.).

7-References

Abkarian, M., Loiseau, E., and Massiera, G. (2011). Continuous droplet interface crossing encapsulation (cDICE) for high throughput monodisperse vesicle design. Soft Matter 7, 4610

Adam, G., and Delbrück, M. (1968). Reduction of dimensionality in biological diffusion processes. In Structural Chemistry and Molecular Biology, (San Francisco: W. H. Freeman and Co.), pp. 198–215

Akhmanova, A. & Steinmetz, M. O. Tracking the ends: a dynamic protein network controls the fate of microtubule tips. Nat. Rev. Mol. Cell Biol. , 309–322 (2008).

Akhmanova, A., and Hoogenraad, C. C. (2005). Microtubule plus-end-tracking proteins: mechanisms and functions. Curr. Opin. Cell Biol. 17, 47–54.

Akhmanova, A., and Steinmetz, M. O. (2011) Microtubule end binding: EBs sense the guanine nucleotide state. Curr. Biol. 21, R283–R285

Alberts B., A. Johnson, J. Lewis, K. Roberts, and P. Walter, ―Molecular Biology of the Cell,‖ pp. 195 – 262, 2008

Amayed P, Pantaloni D, Carlier MF (2002) The effect of stathmin phosphorylation on microtubule assembly depends on tubulin critical concentration. J Biol Chem 277 , 22 718 – 22 724.

Andersen, S.S.L., A.J. Ashford, R. Tournebize, O. Gavet, A. Sobel, A.A. Hy- man, and E. Karsenti. 1997. Mitotic chromatin regulates phosphorylation of Stathmin/Op18. Nature. 389:640–643.

Anne M¨usch. Microtubule organization and function in epithelial cells. Traffic, 51:1–9, Jan 2004., Sarah E Siegrist and Chris Q Doe. Microtubule-induced cortical cell polarity. Genes Dev, 215:483–496, Mar 2007

Bastiaens, P., Caudron, M., Niethammer, P., and Karsenti, E. (2006). Gradients in the selforganization of the mitotic spindle. Trends Cell Biol. 16, 125–134

Baumann, H., and Surrey, T. (2014). Motor-mediated cortical versus astral microtubule organization in lipid-monolayered droplets. J. Biol. Chem. 289, 22524–22535

Belmont LD, Mitchison TJ (1996) Identification of a protein that interacts with tubulin dimers and increases the catastrophe rate of microtu- bules. Cell 84:623 – 631

Bieling, P., Telley, I.A., Hentrich, C., Piehler, J., and Surrey, T. (2010). Fluorescence microscopy assays on chemically functionalized surfaces for quantitative imaging of microtubule, motor, and +TIP dynamics. Methods Cell Biol. 95, 555–580

Bo Segerman. Per Holmfeldt. Justin Morabito. Martin Hans Gullberg. Autonomous and phosphorylation-responsive microtubule-regulating activities of the N-terminus of Op18/stathmin. February 2003Journal of Cell Science

Boesze K. - Battaglia and R. J. Schimmel, —Cell membrane lipid composition and distribution: implications for cell function and lessons learned from photoreceptors and platelets,‖ J. Exp. Biol. , vol. 200, no. Pt 23, pp. 2927 – 2936, 1997

Bornens, M., and Moudjou, M. (1999). Studying the composition and function of centrosomes in vertebrates. Methods Cell Biol. 61, 13–34

Brattsand G, Roos G, Marklund U, Ueda H, Landberg G, Nanberg E, Sideras P and Gullberg M (1993) Quantitative analysis of the expression and regulation of an

activation-regulated phosphoprotein (oncoprotein 18) in normal and neoplastic cells. Leukemia 7 : 569–579

Carazo-Salas, R.E.; Guarguaglini, G.; Gruss, O.J.; Segref, A.; Karsenti, E.; Mattaj, I.W. Generation of GTP-bound ran by RCC1 is required for chromatin-induced mitotic spindle formation.Nature 1999 , 400 , 178–181

Carlier M. F. and D. Pantaloni. Kinetic analysis of guanosine 5'-triphosphate hydrolysis associated with tubulin polymerization. Biochemistry, 207:1918–1924, Mar 1981

Cassimeris L (2002) The oncoprotein 18/stathmin family of micro- tubule destabilizers. Curr Opin Cell Biol 14:18–24

Castoldi, M., and Popov, A.V. (2003). Purification of brain tubulin through two cycles of polymerization-depolymerization in a high-molarity buffer. Protein Expr. Purif. 32, 83–88

Maïwen Caudron, Gertrude Bunt, Philippe Bastiaens, Eric Karsenti, Spatial Coordination of Spindle Assembly by Chromosome-Mediated Signaling Gradients. Science 26 Aug 2005: Vol. 309, Issue 5739, pp. 1373-1376

Cho W. and R. V. Stahelin. "Membrane-protein interactions in cell signaling and membrane trafficking". In: Annu Rev Biophys Biomol Struct 34 2005, pp. 119–151. doi : 10.1146/annurev.biophys.33.110502.133337

Conde C, Cáceres A. Microtubule assembly, organization and dynamics in axons and dendrites. Nat Rev Neurosci. 2009 May;10(5):319-32. doi: 10.1038/nrn2631.

Coskun Ü. and K. Simons, —Cell membranes: The lipid perspective,‖ Structure , vol. 19, no. 11, pp. 1543 – 1548, 2011

Cowin P. and B. Burke, —Cytoskeleton – membrane e interactions,‖ Curr. Opin. Cell Biol. , vol. 8, no. 1, pp. 56 – 65, 1996

Curmi, P.A., Andersen, S.S., Lachkar, S., Gavet, O., Karsenti, E., Knossow, M., and Sobel, A. (1997). The stathmin/tubulin interaction in vitro. J. Biol. Chem. 272, 25029–25036

Daub, H., Gevaert, K., Vandekerckhove, J., Sobel, A., and Hall, A. (2001). Rac/Cdc42 and p65PAK regulate the microtubule-destabilizing protein stathmin through phosphorylation at serine 16. J. Biol. Chem. 276, 1677–1680

Dehmelt L, Halpain S. Actin and microtubules in neurite initiation: are MAPs the missing link?. J Neurobiol. 2004 Jan;58(1):18-33.

Deneubourg JL (1977). Application de l'ordre par fluctuations à la description de certaines étapes de la construction du nid chez les termites. Insectes Sociaux, 24, 117-130

Desai, A., and Mitchison, T. J. (1997) Microtubule polymerization dynamics .Annu. Rev. Cell Dev. Biol. 13, 83–117

Di Paolo, A. and T. J. Mitchison (1997).

Downing, K. & Nogales, E. Eur Biophys J (1998) 27: 431.

Elodie Charbaut, Patrick A. Curmi, Sylvie Ozon, Sylvie Lachkar, Virginie Redeker and André Sobel. Stathmin Family Proteins Display Specific Molecular and Tubulin Binding Properties. May 11, 2001 The Journal of Biological Chemistry 276, 16146-16154.

Fygenson, Braun, and Libchaber. Phase diagram of microtubules. Physical Review. E. Statistical Physics, Plasmas, Fluids, and Related Interdisciplinary Topics, 502:1579–1588, Aug 1994

Gardner, M.K., Zanic, M., Gell, C., Bormuth, V., and Howard, J. (2011). Depolymerizing kinesins Kip3 and MCAK shape cellular microtubule architecture by differential control of catastrophe. Cell 147, 1092–1103

Gigant B, Curmi PA, Martin-Barbey C, Charbaut E, Lachkar S, Lebeau L, Siavoshian S, Sobel A, Knossow M. The 4 A X-ray structure of a tubulin:stathmin-like domain complex. Cell. 2000 Sep 15;102(6):809-16.

Head B. P. , H. H. Patel, and P. a. Insel, —Interaction of membrane/lipid rafts with the cytoskeleton: Impact on signaling and function: Membrane/lipid rafts, mediators of cytoskeletal arrangement and cell signaling,‖ Biochim. Biophys. Acta - Biomembr. , vol. 1838, no. 2, pp. 532 – 545, 2014

Hill T. L. . Theoretical problems related to the attachment of microtubules to kinetochores. Proc Natl Acad Sci U S A, 8213:4404–4408, Jul 1985

Hirokawa N, Niwa S, Tanaka Y. Molecular motors in neurons: transport mechanisms and roles in brain function, development, and disease. Neuron. 2010 Nov 18;68(4):610-38. doi: 10.1016/j.neuron.2010.09.039.

Hirokawa N. Kinesin and dynein superfamily proteins and the mechanism of organelle transport. Science. 1998 Jan 23;279(5350):519-26.

Holy T. E. and S. Leibler. Dynamic instability of microtubules as an efficient way to search in space. Proc Natl Acad Sci U S A, 9112:5682–5685, Jun 1994

Howell, B., Larsson, N., Gullberg, M., and Cassimeris, L. (1999). Dissociation of the tubulin-sequestering and microtubule catastrophe-promoting activities of oncoprotein 18/stathmin. Mol. Biol. Cell 10, 105–118

Hyman A., S. Salser, D. N. Drechsel, N. Unwin, and T. J. Mitchison. Role of GTP hydrolysis in microtubule dynamics: information from a slowly hydrolyzable analogue, GMPCPP. Mol Biol Cell, 310:1155–1167, Oct 1992

Inou ´ e S. 1951. A method for measuring small retardations of structures in living cells. Exp. Cell Res. 2:513–17

Ioan Susnea, Cristian Axenie. Cognitive Maps for Indirect Coordination of Intelligent Agents. March 2015Studies in Informatics and Control 24(1):111-118

James Tabony. Microtubules viewed as molecular ant colonies. 2006 Société Française des Microscopies and Société Biologie Cellulaire de France

Jourdain, L., Curmi, P., Sobel, A., Pantaloni, D., and Carlier, M.F. (1997). Stathmin: a tubulinsequestering protein which forms a ternary T2S complex with two tubulin molecules. Biochemistry 36, 10817–10821.

Juliane P.CavistonErika L.F.Holzbaur, Microtubule motors at the intersection of trafficking and transport, Trends Cell Biol. 2006 Oct;16(10):530-7. Epub 2006 Aug 30.

Juniper, M.P.N., Weiss, M., Platzman, I., Spatz, J.P., and Surrey, T. (2018). Spherical network contraction forms microtubule asters in confinement. Soft Matter 14, 901–909

Kalab, P, RT Pu, and M Dasso. 1999. “The Ran GTPase Regulates Mitotic Spindle Assembly.”. Curr Biol 9: 481 – 84

Kalab,P., Weis,K. and Heald,R. (2002) Visualization of a Ran-GTP gradient in interphase and mitotic Xenopus egg extracts. Science , 295 , 2452±2456

Keren K. “Cell motility: the integrating role of the plasma membrane”. In: Eur. Biophys. J. 40.9 2011, pp. 1013–1027. doi : 10.1007/s00249 011-0741-0

Laan, L., Roth, S., and Dogterom, M. (2012). End-on microtubule-dynein interactions and pulling-based positioning of microtubule organizing centers. Cell Cycle Georget. Tex 11, 3750–3757

Larsson T, et al. (1997) Identification of two-dimensional gel electrophoresis resolved yeast proteins by matrix-assisted laser desorption ionization mass spectrometry. Electrophoresis 18(3-4):418-23

Letort, G., Nedelec, F., Blanchoin, L., and Théry, M. (2016). Centrosome centering and decentering by microtubule network rearrangement. Mol. Biol. Cell 27, 2833–2843

M. O. Steinmetz et al ., EMBO J. 19 , 572 (2000)

Mary Ann Jordan and Leslie Wilson. Microtubules as a target for anticancer drugs. Nat Rev Cancer, 44:253–265, Apr 2004

McPhee C. I. et al. “Measuring the Lamellarity of Giant Lipid Vesicles with Differential Interference Contrast Microscopy”. In: Biophysical Journal 105.6 2013, pp. 1414–1420

Mitchison T. J. and M. W. Kirschner. Dynamic instability of microtubule growth. Nature, 3125991:237–242, 1984., M. F. Carlier and D. Pantaloni. Kinetic analysis of guanosine 5’-triphosphate hydrolysis associated with tubulin polymerization. Biochemistry, 207:1918–1924, Mar 1981

Mitchison, T. & Kirschner, M. W. "Dynamic instability of microtubule growth" Nature 312, 237–242 (1984)

Montenegro Gouveia S, Leslie K, Kapitein LC, Buey RM, Grigoriev I, Wagenbach M, Smal I, Meijering E, Hoogenraad CC, Wordeman L, Steinmetz MO, Akhmanova A. In vitro reconstitution of the functional interplay between MCAK and EB3 at microtubule plus ends. Curr Biol. 2010 Oct 12;20(19):1717-22. doi: 10.1016/j.cub.2010.08.020. Epub 2010 Sep 16.

Mueller P. , T. F. Chien, and B. Rudy. “Formation and properties of cell-size lipid bilayer vesicles.” In: Biophysical Journal 44.3 1983, pp. 375–381

Nédélec, F.J., Surrey, T., Maggs, A.C., and Leibler, S. (1997). Self-organization of microtubules and motors. Nature 389, 305–308

Neukirchen D, Bradke F. Neuronal polarization and the cytoskeleton. Semin Cell Dev Biol. 2011 Oct;22(8):825-33. doi: 10.1016/j.semcdb.2011.08.007. Epub 2011 Aug 22.

Niethammer, P., Bastiaens, P., and Karsenti, E. (2004). Stathmin-tubulin interaction gradients in motile and mitotic cells. Science 303, 1862–1866

Niethammer, P., Kronja, I., Kandels-Lewis, S., Rybina, S., Bastiaens, P., and Karsenti, E. (2007). Discrete states of a protein interaction network govern interphase and mitotic microtubule dynamics. PLoS Biol. 5, e29

Nogales E. , K. H. Downing, L. A. Amos, and J. L¨owe. Tubulin and ftsz form a distinct family of gtpases. Nat Struct Biol, 56:451–458, Jun 1998

Nogales E. and Hong-Wei Wang. Structural mechanisms underlying nucleotide-dependent self-assembly of tubulin and its relatives. Curr Opin Struct Biol, 162:221–229, Apr 2006

Nogales E. Structural insights into microtubule function. Annu Rev Biochem. 2000;69:277-302.

Oancea, E., and Meyer, T. (1998). Protein kinase C as a molecular machine for decoding calcium and diacylglycerol signals. Cell 95, 307–318

Per Holmfeldt, Niklas Larsson, Bo Segerman, Bonnie Howell, Justin Morabito, Lynne Cassimeris, and Martin Gullberg, The Catastrophe-promoting Activity of

Ectopic Op18/Stathmin Is Required for Disruption of Mitotic Spindles But Not Interphase Microtubules, Mol Biol Cell. 2001 Jan; 12(1): 73–83.
Pigino G, Paglini G, Ulloa L, Avila J, C aceres A (1997) Analysis of the expression, distribution, and f unction of cyclin-dependent kinase 5 (cdk5) in developing cerebellar macroneurons. J C ell Sci 110:257–270

pinot M, Chesnel F, et al. Effects of confinment on the self-organization of microtubules and motors. Current Biology. 2009

Priya Prakash Budde, Akiko Kumagai, William G. Dunphy, and Rebecca Healda, Regulation of Op18 during Spindle Assembly in Xenopus Egg Extracts. J Cell Biol. 2001 Apr 2; 153(1): 149–158.

R Tournebize, S S Andersen, F Verde, M Dorée, E Karsenti, and A A Hyman. Distinct roles of PP1 and PP2A-like phosphatases in control of microtubule dynamics during mitosis. EMBO J. 1997 Sep 15; 16(18): 5537–5549

Rangamani, P., Lipshtat, A., Azeloglu, E.U., Calizo, R.C., Hu, M., Ghassemi, S., Hone, J., Scarlata, S., Neves, S.R., and Iyengar, R. (2013). Decoding information in cell shape. Cell 154, 1356–1369

Raspopovic, J., Marcon, L., Russo, L., and Sharpe, J. (2014). Modeling digits. Digit patterning is controlled by a Bmp-Sox9-Wnt Turing network modulated by morphogen gradients. Science 345, 566–570

Reitsma S. , D. W. Slaaf, H. Vink, M. a M. J. van Zandvoort, and M. G. a oude Egbrink, —The endothelial glycocalyx: composition, functions, and visualization.‖ Pflugers Arch. , vol. 454, no. 3, pp. 345 – 59, 2007

Roger S. L. and V. I. Gelfand. Membrane trafficking, organelle transport, and the cytoskeleton. Curr Opin Cell Biol, 121:57–62, Feb 2000

Schmick, M., and Bastiaens, P.I.H. (2014). The interdependence of membrane shape and cellular signal processing. Cell 156, 1132–1138
Schmidt, W.J. 1939. Doppelbrechung der Kernspin- del und Zugfasertheorie der Chromosomenbewe- gung. Chromosoma. 1:253–264

Schmitt C. et al. “Compartmentalization and Transport in Synthetic Vesi- cles”. In: Frontiers in Bioengineering and Biotechnology 4 2016, p. 19

Sean Lawler, Olivier Gavet, Tina Rich, André Sobel, Stathmin overexpression in 293 cells affects signal transduction and cell growth. FEBS Letters 421 (1998) 1873-3468

Shen K, Meyer T. Dynamic control of CaMKII translocation and localization in hippocampal neurons by NMDA receptor stimulation. Science. 1999 Apr 2;284(5411):162-6.

Surrey T, Nedelec F, Leibler S, Karsenti E. Physical properties determining self-organization of motors and microtubules. Science. 2001 May 11;292(5519):1167-71.

Susan L Kline-Smith and Claire E Walczak. Mitotic spindle assembly and chromosome segregation: refocusing on microtubule dynamics. Mol Cell, 153:317–327, Aug 2004

Theraulaz, G., Gautrais, J., Camazine, S., and Deneubourg, J.-L. (2003). The formation of spatial patterns in social insects: from simple behaviours to complex structures. Philos. Transact. A Math. Phys. Eng. Sci. 361, 1263–1282
U. Marklund, N. Larsson, H. M. Gradin, G. Brattsand,M. Gullberg, EMBO J. 15 , 5290 (1996).

van Meer G. , D. R. Voelker, and G. W. Feigenson, —Membrane lipids: where they are and how they behave,|| Nat. Rev. Mol. Cell Biol. , vol. 9, no. 2, pp. 112 – 124, 2008

Verhey KJ, Gaertig J. The tubulin code. Cell Cycle. 2007 Sep 1;6(17):2152-60. Epub 2007 Jun 26.

Walde P. et al. “Giant Vesicles: Preparations and Applications”. In:ChemBioChem 11.7 2010, pp. 848–865

Walker RA, O'Brien ET, Pryer NK, Soboeiro MF, Voter WA, Erickson HP, Salmon ED. Dynamic instability of individual microtubules analyzed by video light microscopy: rate constants and transition frequencies. J Cell Biol. 1988 Oct;107(4):1437-48.

Wallon G, Rappsilber J, Mann M, Serrano L. Model for stathmin/OP18 binding to tubulin. EMBO J. 2000 Jan 17;19(2):213-22.

Weinbaum S, J. M. Tarbell, and E. R. Damiano, —The structure and function of the endothelial glycocalyx layer.,‖ Annu. Rev. Biomed. Eng. , vol. 9, pp. 121 – 167, 2007

Wilson L, Jordan MA. New microtubule/tubulin-targeted anticancer drugs and novel chemotherapeutic strategies. J Chemother. 2004 Nov;16 Suppl 4:83-5.

Wollman R., E. N. Cytrynbaum, J. T. Jones, T. Meyer, J. M. Scholey, and A. Mogilner. Efficient chromosome capture requires a bias in the ’search-andcapture’ process during mitotic-spindle assembly. Curr Biol, 159:828–832, May 2005

8-Acknowledgement

First, I would like to thank Prof. Dr. Philippe Bastiaens for giving me not only a great opportunity to work on an interesting and exciting project, but also for his scientific guidance and constructive criticism. I would like also to thank Dr. Aneta Koseska for valuable suggestions and scientific discussions.

I am thankful to Dr. Astrid Krämer, Tanja Forck, Kristen Michel and Hendrike Schütz who has been always there to help me with my problems.

It would have been impossible to do what I have done without Dr. Konstantin Gavriljuk. He helped me a lot during my PhD and he is a great friend, brother and colleague. thank you.

I want to thank my colleagues and friends who helped me with data analysis and helpful discussion; Bruno, Akhilesh, Manuel and Hans.

I want to thank my “Hombruch Boyz”, Wayne, Amit, Angel, Andrej and Dhruv for having a great and fun time together.

I would further like to thank all current and past members of Department 2, that are not mentioned by name, for all the good times, the help and discussions.

And last but not least, my special thanks goes to my family; mom and dad, thanks for being an amazing inspiration, thanks for being a great support, thanks for the love. Also not to forget, I have to thank my brother, Omid, and my lovely sister, Farzaneh. I have to say to my family, without you, nothing was possible.

Thanks,
Farid